UNIVERSITY OF HAWAII
INSTITUTE FOR ASTRONOMY
2680 Woodlawn Drive
Honolulu, Hawaii 96822

NASA GRANT NGL 12-001-057

SEMIANNUAL PROGRESS REPORT #25

John T. Jefferies, Principal Investigator

For the Period

July-December 1982

TABLE OF CONTENTS

I. PERSONNEL

This report covers the period July-December 1982. Scientific personnel engaged in planetary research who were supported fully or in part by this grant during the period are:

W. M. Sinton	D. Morrison	C. B. Pilcher
D. P. Cruikshank	J. Goguen	R. R. Howell

In addition, graduate students D. Backman and J. F. Morgan received salary support on research assistantships. A summer student, G. S. Aldering, was also supported through this grant.

II. THE RESEARCH PROGRAMS

A. HIGHLIGHTS

1. First ground-based detection of east-west (local time) asymmetries in the Jovian torus.
2. New three-dimensional models of the plasma conditions in the Jovian torus based on images of the SII emission.
3. Development of a plasma-wind sweeping model to account for sodium directional features emanating from Io.
4. Detection of rotational variations in methane-band images of Neptune acquired with the CCD camera.
5. Discovery that Io's rapid flickering, night-to-night fluctuation, and fluctuation on both longer and shorter periods agree with a fluctuation power spectrum that varies inversely with frequency.
6. Conclusion that improved thermophysical models that include rotation effects and horizontal inhomogeneities are necessary for the proper interpretation of the Io eclipse observations obtained by Sinton and Kaminski at the IRTF.
7. Determination of the diameters and albedos of the satellites of Uranus from radiometric observations.
8. Establishment of significant upper limits to the diameters of Pluto and Triton from radiometric observations.
9. Completion of a network of standard stars for photometric studies in the mid-infrared.

B. THE MAJOR PLANETS

1. Jovian Magnetospheric Studies

We have completed the reduction of all of our 1981 SII images of the plasma, and have made substantial progress on a detailed modeling study aimed at an understanding of the plasma conditions based on these data. The data reduction was accomplished by Research Associate Fertel working under Pilcher's supervision. Fertel also adapted the graphics program written by Morgan for the torus movie in order to use it on the Institute's IIS image processing system. In examining the data in this way, Fertel and Pilcher have found systematic east/west variations in the torus properties as well as variations with magnetic longitude. The first indication of systematic east/west variations in the ground-based data came not from the images, but from the low-resolution spectra acquired by Morgan for his dissertation (see below). In the images these variations manifest themselves in two ways. First, the field-aligned feature (FAF) is systematically 0.2-0.4 R_J further from Jupiter to the east than to the west. Second, the tilt of the torus appears to be 1-2° less to the east than to the west. An offset of the data to the south, generally necessary to match all of the images of a given night with a single tilt angle, is generally smaller to the east than to the west.

These results suggest that we are seeing a manifestation of the dawn/dusk intensity variation seen in SIII EUV emission detected by the Voyager UVS (Sandel and Broadfoot, J. Geophys. Res. 87, 212, 1981). In an explanation of this EUV variation, Barbosa and Kivelson (submitted to Geophys. Res. Lett.) predicted that ions should be farther from Jupiter at local dawn than at local dusk, in accordance with our observations.

Superimposed on the east/west variations are variations with magnetic longitude. Both the intensity and radial distance of the FAF seem to vary in

this manner. We believe that with our ability to separate these two types of variations we are approaching a more accurate description of the torus phenomenology than has been developed previously. Through our modeling program we are also developing an understanding of the plasma characteristics that underlie this phenomenology.

In Figure 1, we show a comparison between an image from the movie acquired at a magnetic longitude near that of the north magnetic pole and the results of a model calculation for the corresponding viewing geometry. The model emission is calculated in three dimensions and then projected onto the plane of the sky for comparison with the observations. The program, written by Morgan, accepts as input arbitrary functions representing the variations of plasma parameters (electron density and temperature, ion mixing ratio) with zenocentric distance and magnetic longitude. The model of Figure 1b was calculated for a longitude-invariant torus. The radial functions used are shown in Figures 2a-c. These functions were derived from Voyager in situ data, but differ in significant ways required by the observations. For example, the plasma temperatures shown in Figure 2c are generally lower than the corresponding ion temperatures reported by Bagenal and Sullivan (J. Geophys. Res. 86, 8447, 1981), the difference reaching a factor of 3 at distances greater than 6 R_J. The higher Voyager temperatures are excluded by the height of the FAF along the field lines. Another difference is the radial distance of the inner peak in the electron density distribution (Fig. 2a).

Although this longitude-invariant model provides a good match to the image shown, other images require variations in the plasma properties with longitude. This is consistent with the overall variations with longitude discerned from image to image. We have not yet calculated models for images other than those of the torus movie, but we intend to extend this modeling

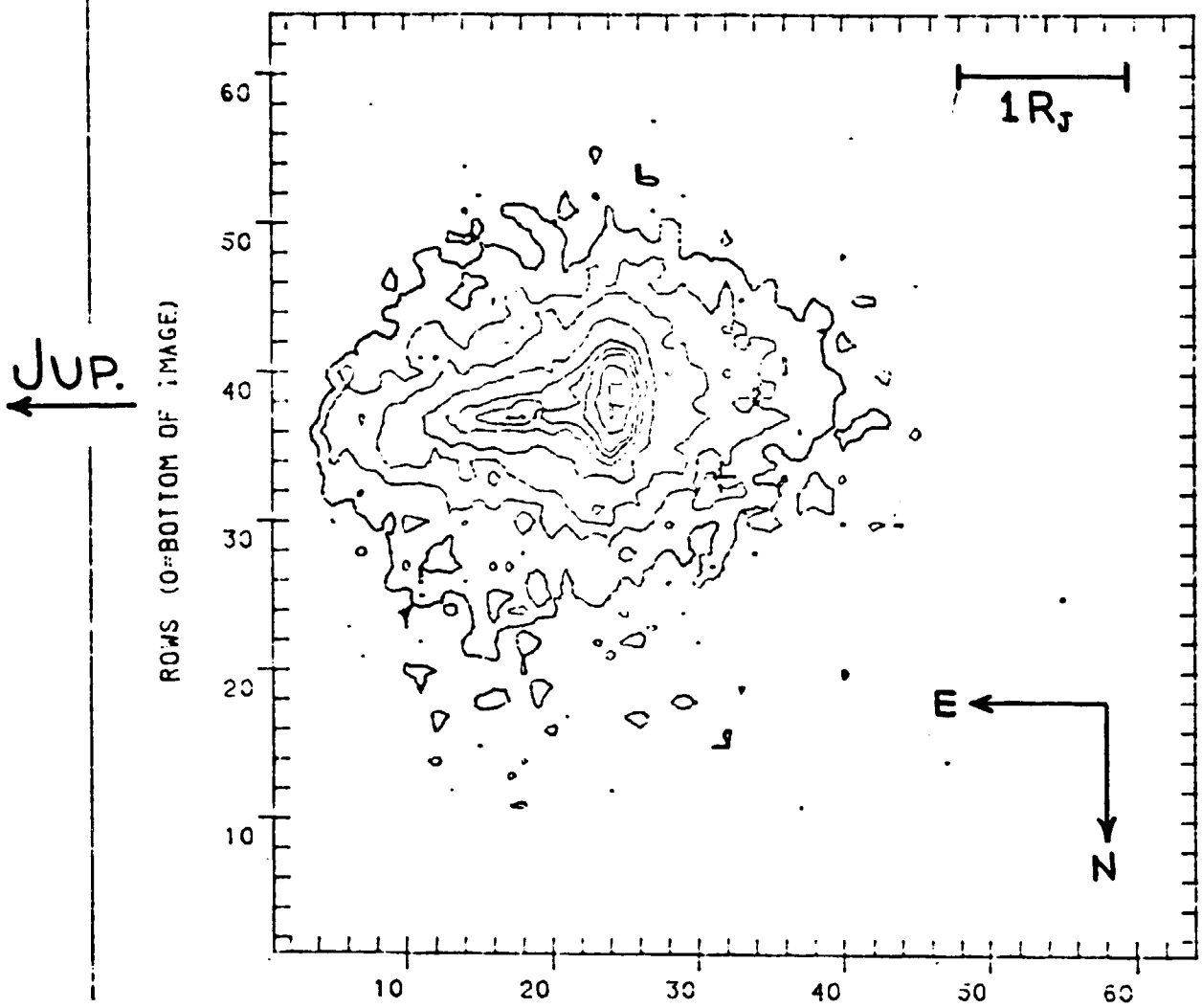

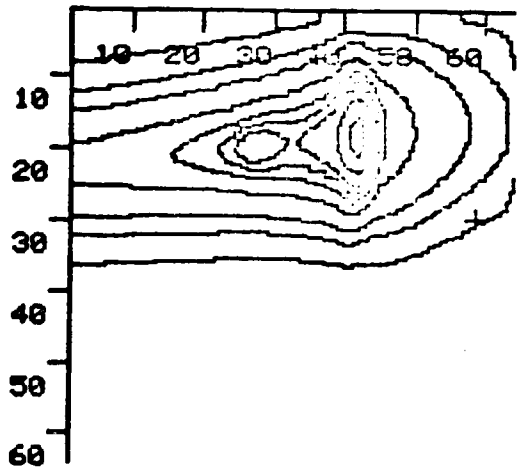

Fig. 1a (top). A contour plot of an image of the Io torus obtained in the light of [SII] λ6731. The magnetic longitude of the observed torus ansa at the central time of the 10-minute exposure was 168°.

Fig. 1b (bottom). A model of the torus at the same viewing geometry calculated with parameters adjusted to provide a good match to the image.

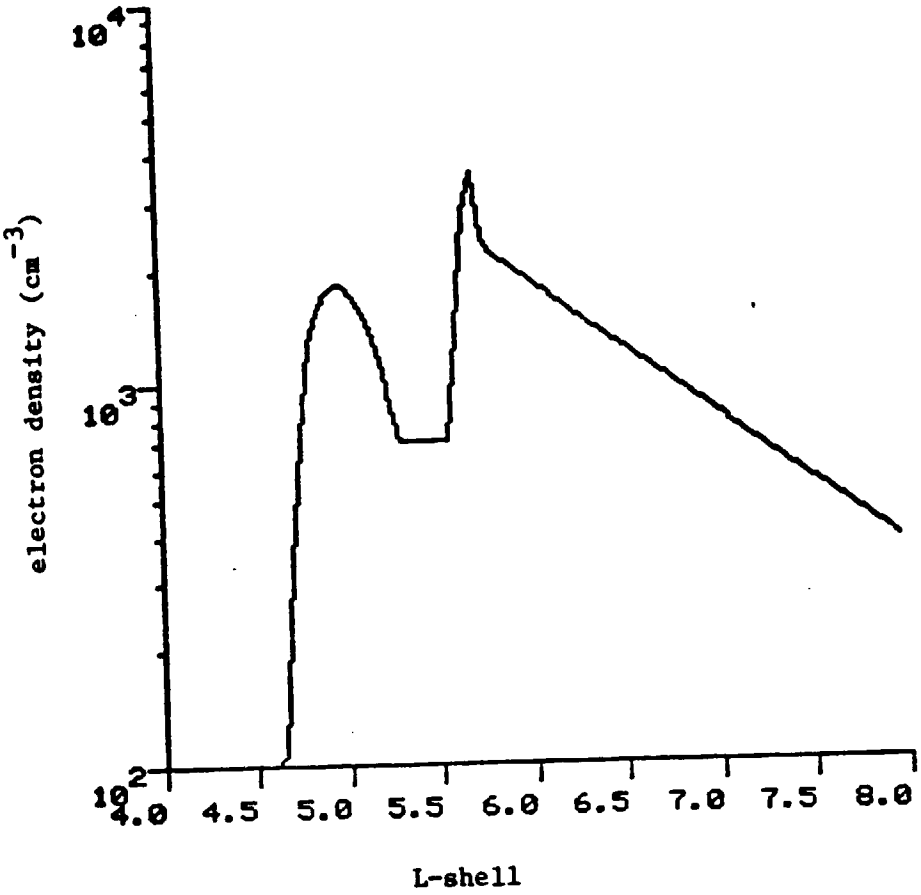

Fig 2a. The radial variation of electron density used for the model of Fig. 1b. The abcissa may be regarded as a scale of distance from the Jovian rotation axis in units of R_J.

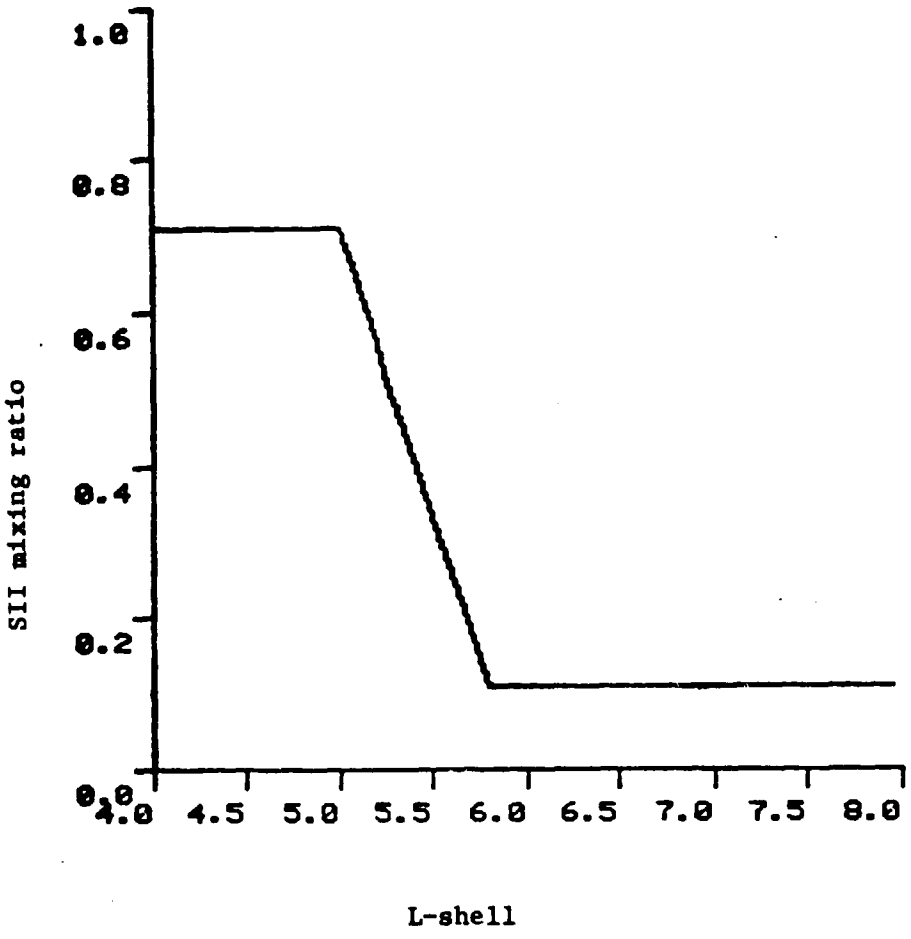

Fig. 2b. As in Fig. 2a, but for the SII mixing ratio.

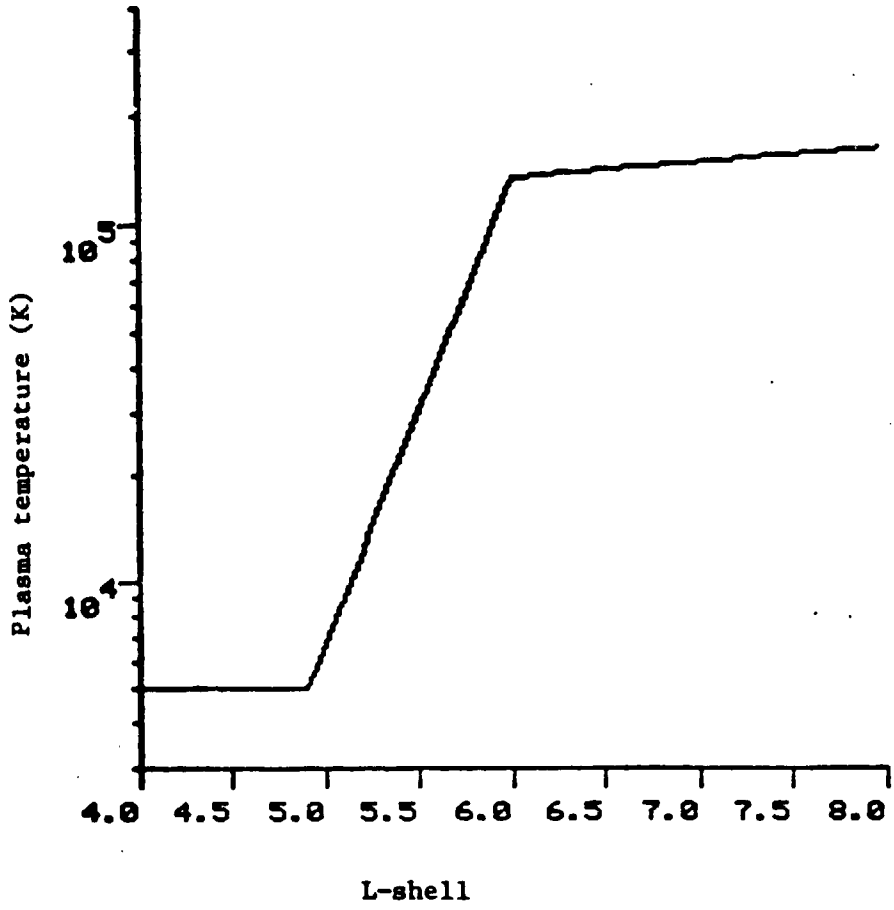

Fig. 2c. As in Fig. 2a, but for the plasma temperature. Electron and ion temperatures were assumed equal.

approach to our entire data set. We hope thereby to gain a detailed understanding of both the temporal and spatial variations of the plasma torus. A paper on the first stage of this process, the analysis of the movie data, is in preparation.

In attempting to understand the origin of the directional features we have observed in Io's sodium cloud, Pilcher and W. H. Smyth of AER, Inc. (Cambridge, MA) have developed a model that may account for the basic features of the data. The model is shown schematically in Figure 3. We assume that sodium atoms are ejected from Io's atmosphere by near-corotating heavy ions in elastic collisions that result from atomic sodium's relatively high polarizability (Brown, Pilcher, and Strobel in Physics of the Jovian Magnetosphere, A. J. Dessler, ed., Cambridge Univ. Press, 1983) For simplicity, we assume that atoms are ejected at a single velocity at an angle η to the local horizontal. Atomic ejection takes place over the entire trailing hemisphere except for a "stagnation" region around the hemisphere's center. The result is a hollow cone of high velocity (~20 km/sec) sodium atoms directed forward from Io and symmetric about the Galilean satellite orbital plane. In the absence of other processes, line of sight effects would make such a cone appear on the sky at two inclined linear features bordering a region of relatively weak emission. However, the response of this distribution to the oscillating plasma torus will significantly affect its appearance.

The lifetime of a sodium atom against electron impact ionization in the densest part of the plasma torus is only 1 to 2 hours. Charge-exchange reactions would lead to an even shorter lifetime. The tilted plasma torus, however, oscillates north-south about Io with a period of 13 hours. During the 4 to 5 hours that the torus is largely, for example, to the north of Io, the atoms in the northern section of the hollow cone become ionized and lost view.

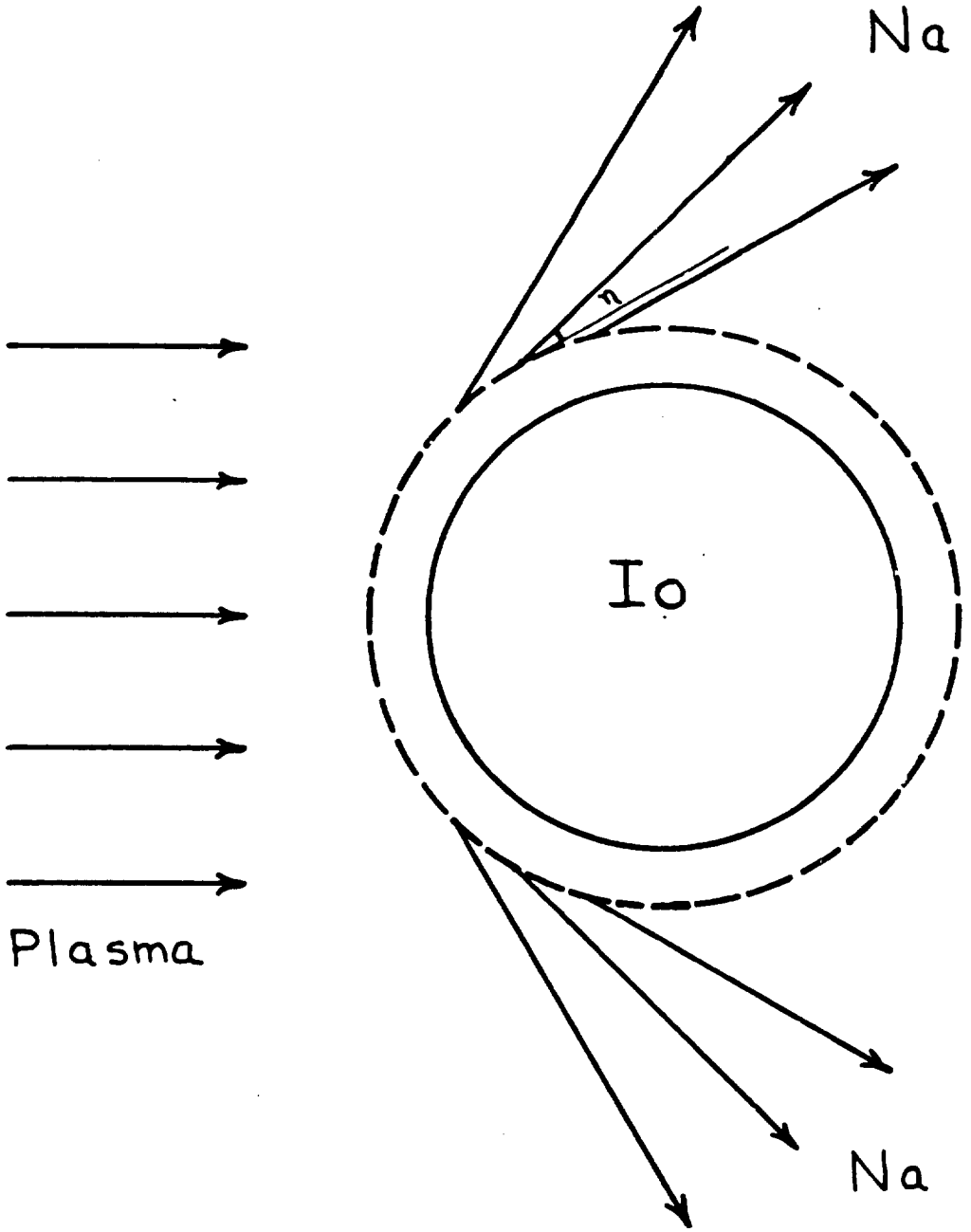

Fig. 3. A schematic diagram of our model of sodium ejection from Io. Corotating heavy ions collide with sodium atoms in Io's atmosphere, ejecting them at an angle n to the local horizontal. The resulting sodium distribution is a hollow cone. In our model, alternating electron-impact ionization of the north and south sides of the cone leads to an apparently single directional feature which oscillates north-south.

The time required to replenish this section of the cone with atoms newly removed from Io is about four hours at our inferred ejection velocity of 20 km/sec. When the torus moves to the south of Io, there is therefore sufficient time for the northern section of the torus to again become prominent. At the same time the southern section diminishes owing to ionization. The result is a single directional feature that appears to oscillate about the Galilean satellite plane.

In Figure 4, we show an example of the results of this model in which the axis of the sodium distribution is clearly inclined with respect to the Galilean satellite orbital plane. However, we have not yet been able to obtain a satisfactory match between the data and the observations. This does not seem to be due to a fundamental weakness of the model, but rather to the large volume of model parameter space that must be investigated. Pilcher and Smyth will continue to pursue this approach. A paper describing the data and their initial modeling efforts is in preparation.

Morgan's dissertation research on the optical emissions from the Io torus has produced several interesting results. This work includes a comparison of the spatial distributions of the oxygen ([OII] λλ3726,3729) and sulfur lines ([SII] λλ6716,6731 and λλ4069,4076). He has completed the first attempt to spatially characterize the oxygen ion emissions. [OII] is found to extend farther out from Jupiter than the [SII] emission. Between 5.5 and 6.0 R_J from Jupiter the full width at half maximum of the sulfur emission was measured to be ~7° of magnetic latitude while the [OII] emission had a width of ~12.5°. No dependence on magnetic longitude was seen in the oxygen emission, although such a dependence was present for sulfur. In general, most of the temporal trends seen in the sulfur emissions were evident in the oxygen data: when the average [SII] ratio 6716/6731 decreased, then so did the average [OII]

SODIUM D2 LINE

1070c

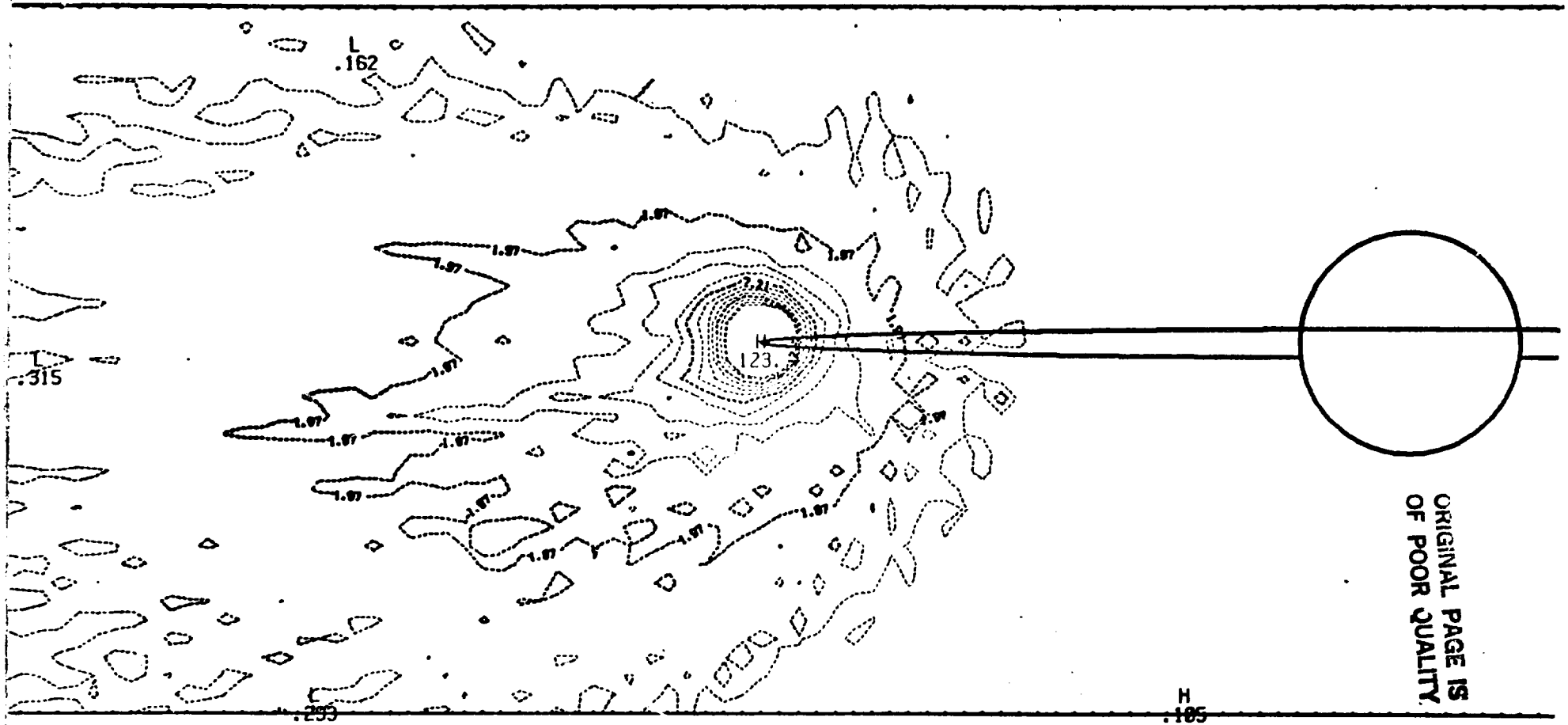

Fig. 4. An example of the results of a calculation based on the model of Fig. 3.

3729/3726 ratio; when the sulfur 6731 intensity increased, so did the oxygen 3726.

All of the emissions showed an east-west asymmetry which had previously been seen only in the Voyager ultraviolet measurements. Figure 5 illustrates how the east-west asymmetry is manifested in the radial distributions of all the emissions. Each graph in Figure 5 is a plot of the emission intensity (y-axis in Rayleighs) as a function of radial distance from Jupiter (x-axis in Jovian radii). The symbols s2r, s2b, and o2 stand for [SII] 6731, [SII] 4069, and [OII] 3726, respectively. The top row consists of measurements made to the east of Jupiter and the bottom row shows data to the west. The eastern emission is fainter and extends to larger zenocentric distances than the western emission. The sulfur and oxygen doublet ratios also showed an east-west asymmetry. The effect was more pronounced in the oxygen ratio. The east and west oxygen ratios were 0.74 ± 0.02 and 0.59 ± 0.02, respectively. The eastern sulfur and oxygen ratios clearly differed by ~0.1, but the western ratios were nearly the same. As reported above, the radial measurements are consistent with Barbosa and Kivelson's prediction. The ratio asymmetries are consistent with a compression of the plasma as it rotates from the east to the west of Jupiter. The 4069/6731 [SII] ratio indicates that the western electron temperature is ~6 eV while in the east it is 1 to 2 eV.

Morgan has also found evidence that the plasma emissions are not centered on the centrifugal equator but lie 0.1-0.2 R_J to the north of this surface. The centrifugal equator is the theoretical equilibrium surface for an ion controlled by a balance of magnetic and centrifugal forces. This offset could be indicative of a northern offset to Jupiter's magnetic field or a manifestation of an electric field anti-parallel to the Jovian magnetic field.

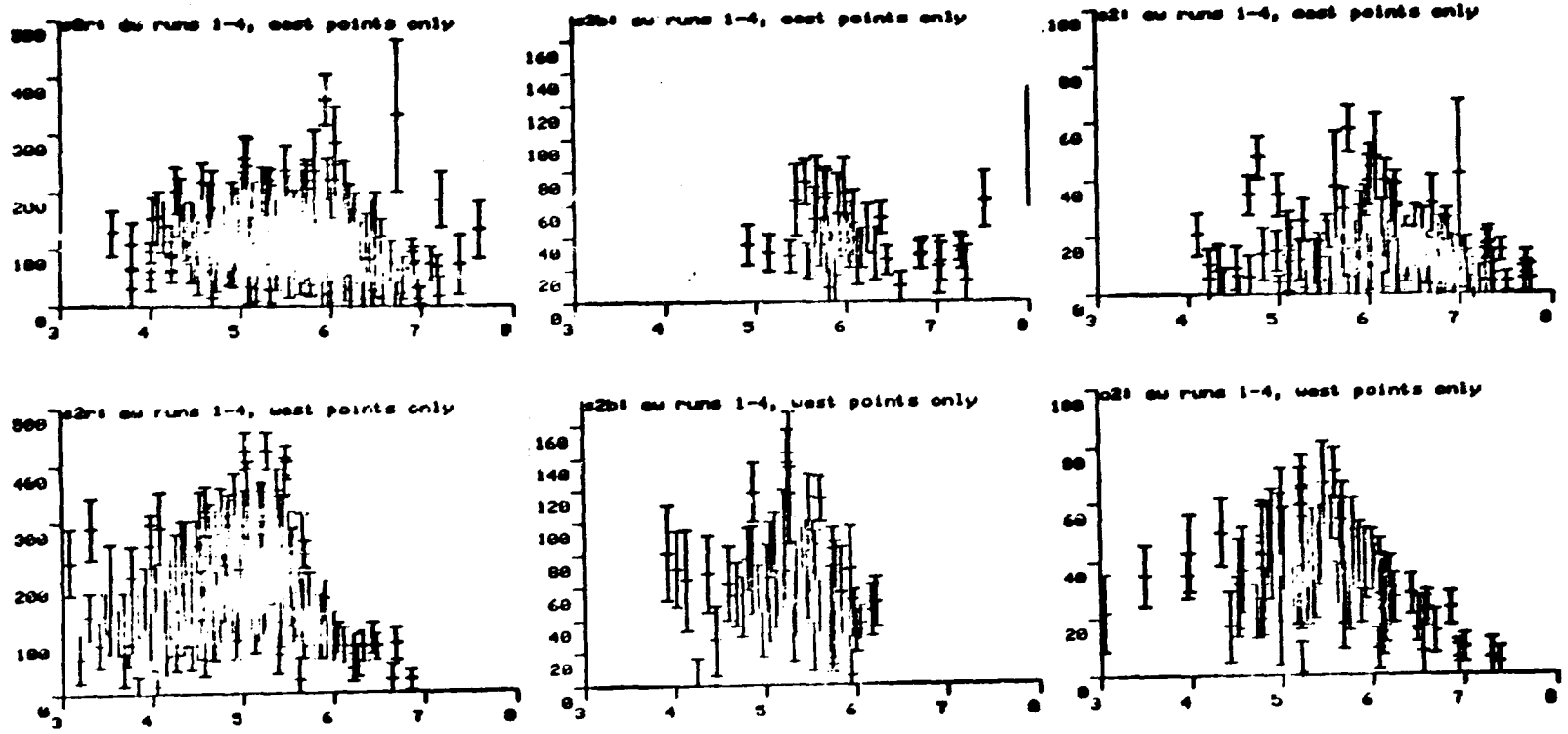

Fig. 5. The maximum emission intensities observed in individual spectra of the plasma. Top: Data obtained to the east of Jupiter. Bottom: Data obtained to the west of Jupiter. Left: [SII] λ6731. Center: [SII] λ4069. Right: [OII] λ3726.

These data include measurements of the [SII] 6716/6731 ratio that lie below the theoretical limit. Theory predicts a high-density asymptotic limit to the ratio which is sensitive only to the ratio of the transition probabilities involved. These transition probabilities are known only from quantum mechanical calculations of the line strengths. Since this [SII] ratio is used as an electron density indicator for many astrophysical plasmas, errors in these atomic parameters will affect many astronomical studies.

2. CCD Studies of the Major Planet Atmospheres

Pilcher has concentrated on the analysis of CCD images of Uranus and Neptune obtained at the 2.24-m telescope during the first half of 1982. He and J. N. Heasley of the Institute's staff have applied image restoration techniques coded by Heasley to the data with interesting results. In Figure 6 (top row) we show three images of Uranus that have been subjected only to standard processing (bias, flat-field correction). The false-color look-up table used for these illustrations is shown at the bottom of Figure 7. As noted in our previous report, the central three-quarters of the planet's disk appears to be of uniform intensity, indicating the presence of substantial limb brightening. The second row shows these images after the application of a low pass filter to remove spatial frequencies not passed by the 1.5-arcsecond seeing. The third and fourth rows show independent restorations for which point spread functions determined from each individual Uranus frame were used. The strong limb brightening inferred from the raw data is apparent.

In Figure 7 (upper left), we show a model of Uranus in which the brightness increases linearly from center to limb by a factor of 2.5. On the upper right, we show the appearance of this model when smeared with an average point spread function and after application of the same low-pass filter used

FIGURE CAPTIONS

Fig. 6. Top row: Three 8900 Å images of Uranus with only standard processing applied. Second row: Low-pass filtered versions of each image. Third row: Restorations of the filtered images by means of Jansson's technique. Bottom row: Restoraticns of the filtered images by means of Lucy's technique.

Fig. 7. Top left: A model of Uranus in which the surface brightness increases linearly from center to limb by a factor of 2.5. Top right: The model after application of the same low-pass filter applied to the data. Center: Reconstruction of the filtered model by means of Jansson's (left) and Lucy's (right) techniques. Bottom: A color bar showing the color look up table used for Figs. 6-9. DN 0 is at the left and DN 255 at the right.

Fig. 8. As in Fig. 6, but for 8900 Å images of Neptune.

Fig. 9. Top left: A model of Neptune in which only two surface brightness levels, differing by a factor of 4, are observed on the disk. The remainder of the figure is analogous to Fig. 7.

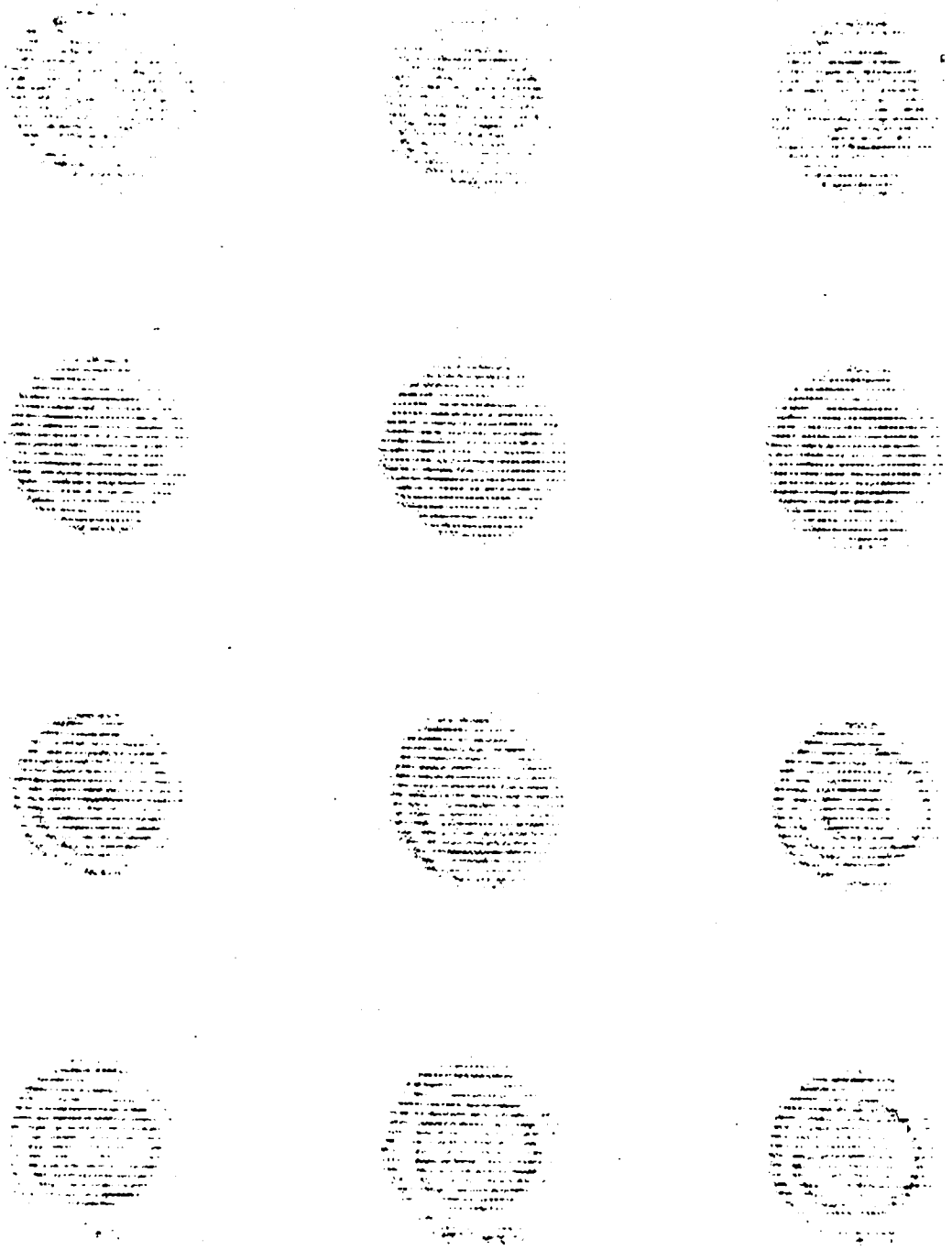

Figure 6

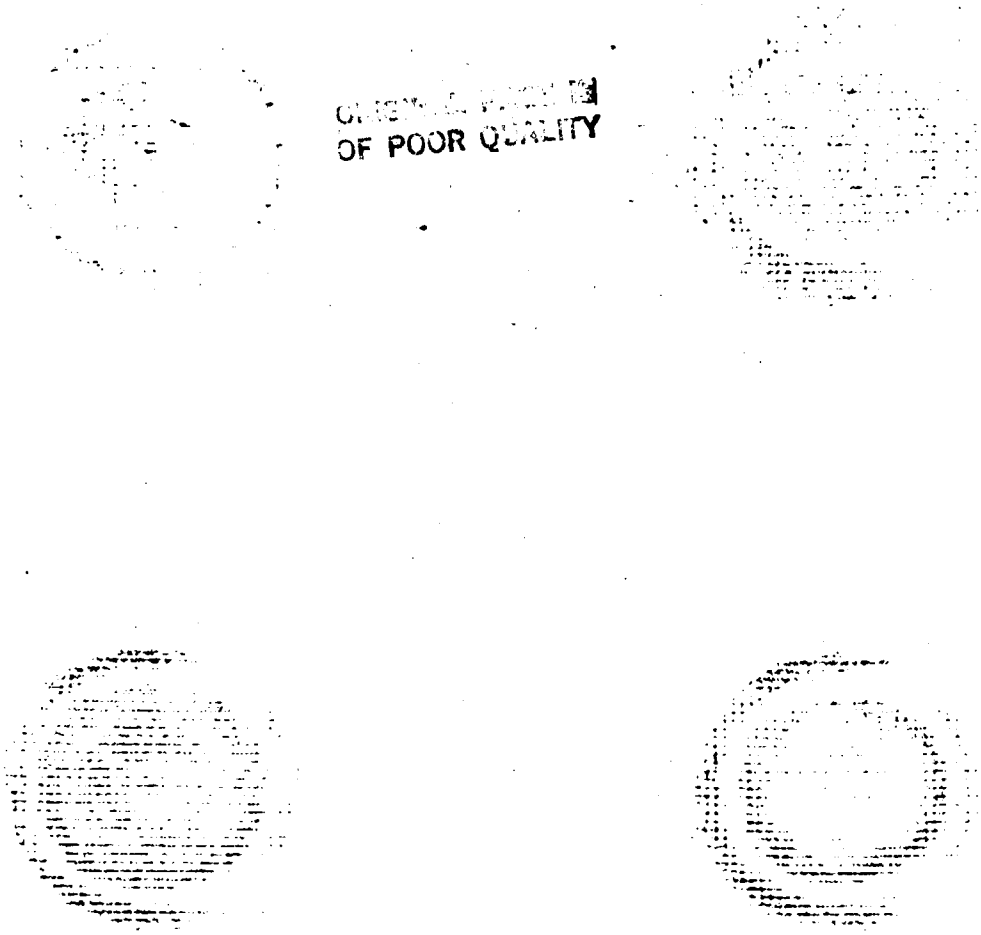

Figure 7

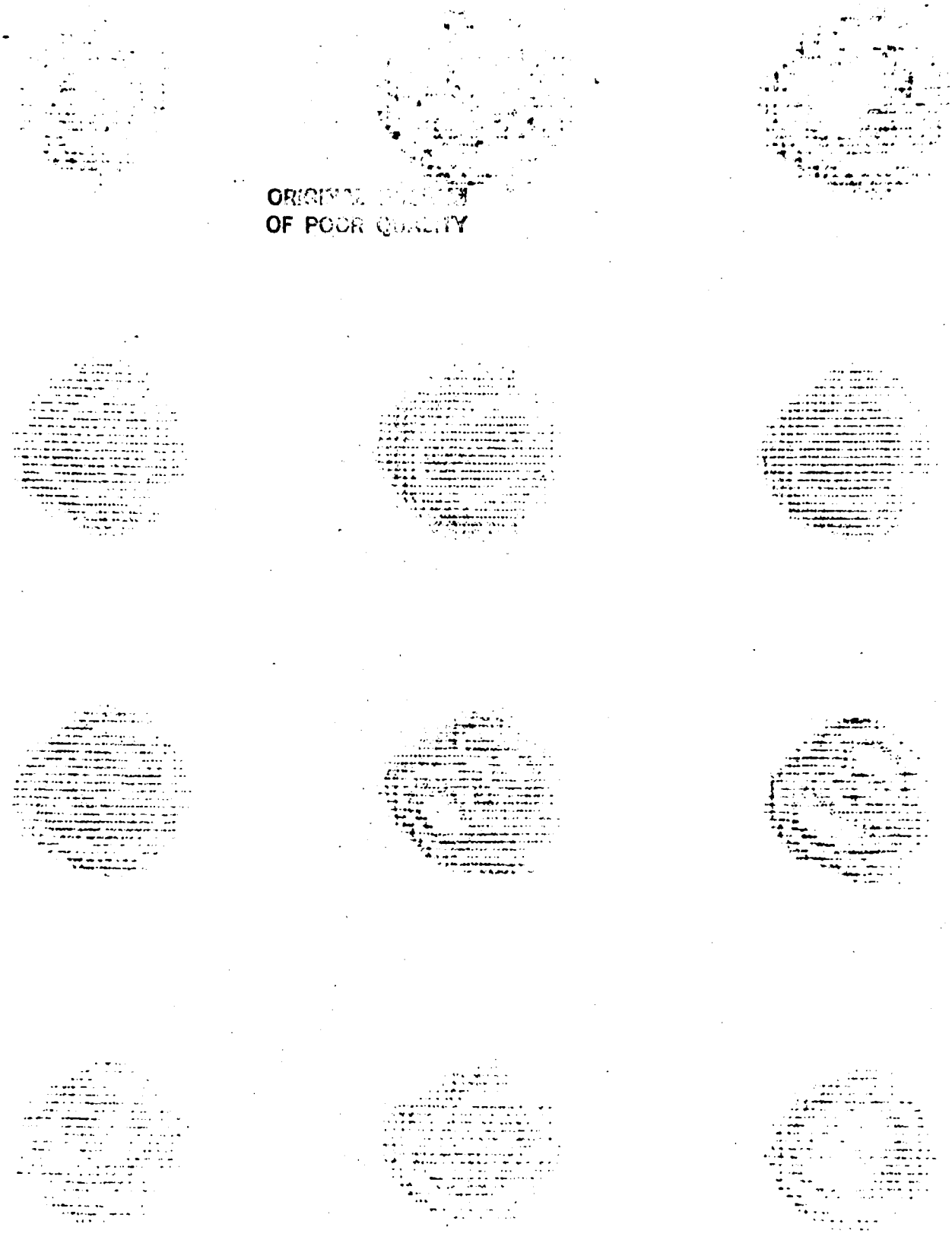

Figure 8

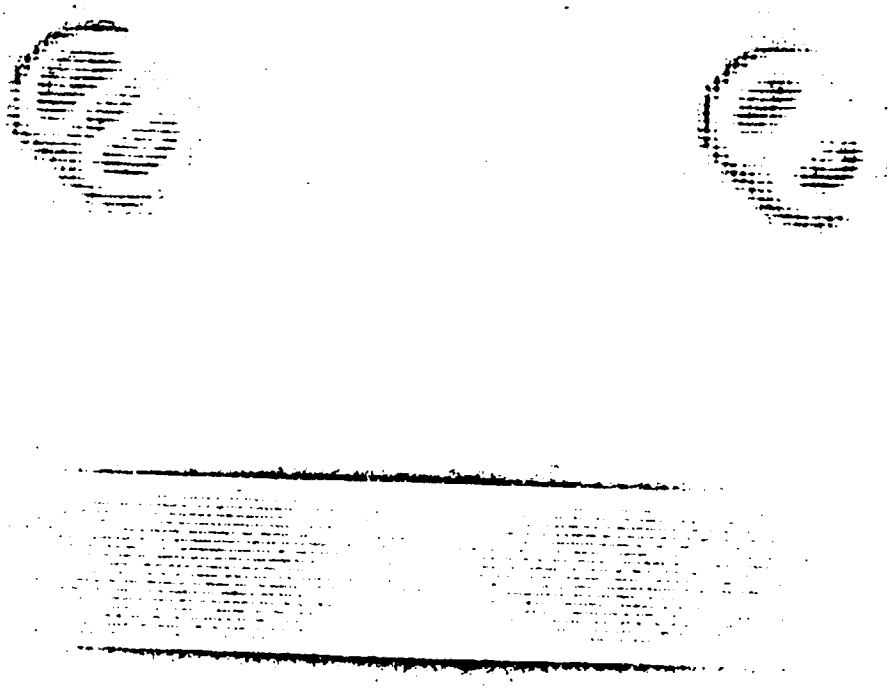

Figure 9

on the data. This simulated observation may be directly compared to the second row of Figure 6. In the bottom row of Figure 7, we show the results of applying the two restoration algorithms to the model. (The lower left image of Figure 7 corresponds to the third row of Figure 6.) As judged from the restorations, the planet seems to be slightly more limb brightened than the model. This may reflect the fact that planets generally exhibit their strongest limb brightening quite close to the limb. Pilcher and Heasley intend to apply these modeling techniques to more realistic center-to-limb profiles to see if an even better match to the data can be obtained.

In Figure 8 we show three Neptune images in the same format. In Figure 9 we show the corresponding model, simulated observation, and restorations. The model shown at the upper left of Figure 9 has only two brightness levels differing by a factor of four. Although the model restorations show the same general characteristics as the restored data, the data all show the southern hemisphere (to the left in Figure 8) to be brighter than the northern. This may be because the subearth latitude on Neptune is currently about $-16°$, exposing more of the bright region around the south pole to our view than that around the north.

It also appears that we are seeing the rotation of Neptune in these data. The right-hand column of Figure 8 shows the first of nine 8900 Å methane band images obtained during a one-hour interval. The center column shows the last of these images. The difference in the brightness distribution on the planet, seen best in the third row, seems to be real and to vary systematically with time. It should be possible to determine whether the apparent rotation rate is consistent with the periods near 18 hours determined by Cruikshank and others, although it will not be possible to obtain a rotation period with high accuracy from these limited data.

A paper on this work is in preparation. These results were presented at the Boulder AAS/DPS meeting in October.

C. SATELLITES AND RINGS

1. Thermal Migration of Water on Ganymede

Pilcher and graduate student E. Shaya have considered the role that thermal migration of water may have played in the delineation of the polar caps on Ganymede. Noting that Callisto does not have polar caps despite having a substantial quantity of surface water, they followed up on a suggestion of N. Purves and Pilcher (Icarus 43, 51, 1980) that Ganymede's polar caps may be the residual of a satellite-wide coating of water ice that formed during a period of geologic activity on Ganymede. This was presumably the period in which the grooved terrain formed as well. Purves and Pilcher advanced this suggestion when they found that thermal migration would not transport water to the poles, and that some other water redistribution mechanism was therefore necessary.

Shaya and Pilcher found that 25 cm is an order-of-magnitude upper limit to the thickness of such an ice layer consistent with its edges having thermally receded to the observed polar cap margins in three billion years. Since this thickness is a factor of ~100 lower than the corresponding gardening depth, it appears that the original supposition of Shaya and Pilcher must be modified. They suggest that the initial thickness of the ice layer was at least several meters. Over time, this ice would have become mixed with the underlying regolith owing to gardening. At equatorial latitudes, the ice in the topmost surface layer has evaporated, leading to the formation of a darker lag deposit. At polar latitudes this surficial ice remains, accounting for the higher polar albedo. One implication of this explanation is that ice sputtering is unimportant for the ice distribution over much, and probably all, of Ganymede.

2. Search for External Rings of Saturn

Low-energy plasma ion density data from Pioneer 11 and Voyagers 1 and 2 (Lazarus et al., submitted to Nature) indicate the probable existence of a faint ring in the Saturn system at ~14 R_S, i.e., between Rhea and Titan. Based on predictions by D. Mink (MIT), Goguen and H. Hammel observed an occultation of SAO 139195 (V ~ 7.6) by the Saturn system on August 14 UT with the 0.6 m telescope and V filter. Observations began during twilight at 15 R_S and continued for ~90 minutes until 21 R_S. Limitations of the data system resulted in ~25 seconds of continuous observations of 0.1 seconds resolution alternating with roughly equal periods of no data corresponding to readout time. Near 15.2 R_S minor intensity variations were observed but are likely due to variations in sky brightness during twilight. Averaged over 50 km intervals in the ring plane, the data indicate no intervals of optical depth $\tau > 0.15$ from 15-21 R_S (~50% coverage).

A second occultation (of SAO 139271, V ~ 8.1) by the Saturn ring plane was observed with both 0.6-m telescopes by Goguen, Cruikshank, and Aldering on September 4 UT. Two continuously recording portable photometers were lent to us by J. Elliot (MIT) and used with filters passing all $\lambda > 0.68$ μm, the red wavelengths selected to minimize atmospheric extinction. Observations began in twilight at ~19 R_S and continued until 15 R_S when Saturn reached too large an airmass for continued observation. Data from both telescopes were combined and compared to those from the August 14 event. No correlation between the two occultations, which covered opposite sides of the planets, was found. The September 4 event shows no evidence for $\tau > 0.15$ from 15-19 R_S (continuous coverage, 50 km width-in-plane average).

The timing of both events was such that we were unable to extend our observations in to 14 R_S, the predicted position of the material. An excellent opportunity to again probe this region occurs in April 1983.

3. 4-μm Spectroscopy of Io

During the second half of 1982 Howell, Cruikshank, and Fanale obtained laboratory spectra of SO_2 in the 4-μm region and used them to interpret recently obtained spectra of Io. The laboratory spectra were produced with the same CVF spectrometer as was used for the astronomical observations, so a precise comparison of wavelength and band shape are possible. The band on Io is in fact virtually identical in shape and wavelength to the frost band, supporting the conclusion that SO_2, not just adsorbed SO_2 gas, is a major component of the surface of Io. Spectra of Io and the frost are shown in Figure __.

The laboratory spectra make it possible to estimate the amount of frost on the satellite's surface. Assuming areal mixtures of frost plus some fairly high albedo neutral component (such as sulfur), the frost must cover more than 50% of the surface; at some longitudes it approaches 100%. The amount of frost is greatest for those longitudes where the white plains unit is most common, but the band is strong enough that frost must be present in other geological units as well.

This is much higher coverage than that estimated by others from ultraviolet observations. The discrepancy can be explained when one considers that in the ultraviolet the frost is bright and sulfur is dark while in the 4-μm band the reverse is true. The apparently contradictory results imply that over much of the surface the frost and the sulfur must be mixed on a scale smaller than the pathlength of a photon. Then at each wavelength the darker component will dominate spectrally, as is the case with the "dirty ice" mixtures on the other Galilean satellites.

These observations restrict models of the transport of the relatively volatile SO_2 on the surface. Those which state that all of the SO_2 cold traps

out on the white plains are too simple. The SO_2 frost must be stable in some form in the darker albedo terrain or the resurfacing must be faster than the time it takes for the SO_2 to sublimate and be transported away. We are currently investigating the implications of these observations for the geology of the satellite.

4. Thermal Studies of Io

Sinton completed observations for this apparition on the monitoring program. Altogether, and including 4 nights when Io was observed out-of-eclipse on the IRTF, useful 4.8-μm observations were obtained on 17 nights despite poor weather during the period. The mean brightness decreased by 20%, continuing an effect noted in Semiannual Report #24. Additional studies were made in July and August to improve the monitoring of Io for variability in sample periods ~10 minutes. This was done because it became apparent that the earlier discovered night-to-night variability, the rapid flickering (~20 seconds), and the now apparent ~20% annual variation are all part of the same fluctuation phenomenon. Sinton, with the assistance of undergraduate W. Tittemore, made a systematic effort to (1) test the significance of the rapid flickering statistically, (2) derive the power spectrum of the rapid flickering, and (3) see if there was a common frequency dependence that linked all of the variable flux phenomena. Such a connection was found, and it now seems clear to us that the power spectrum of the Io 4.8-μm fluctuation varies as the reciprocal of the frequency (Figure 10). A paper on this result has been prepared and submitted to Icarus. Sinton suggests that the physical explanation of the phenomenon may be quite similar to the physical explanation of a similar flicker noise in the emission of electrons from BaO cathodes in electron tubes. If this be true, the ultimate explanation may be due to a correlation between convecting globs of magma

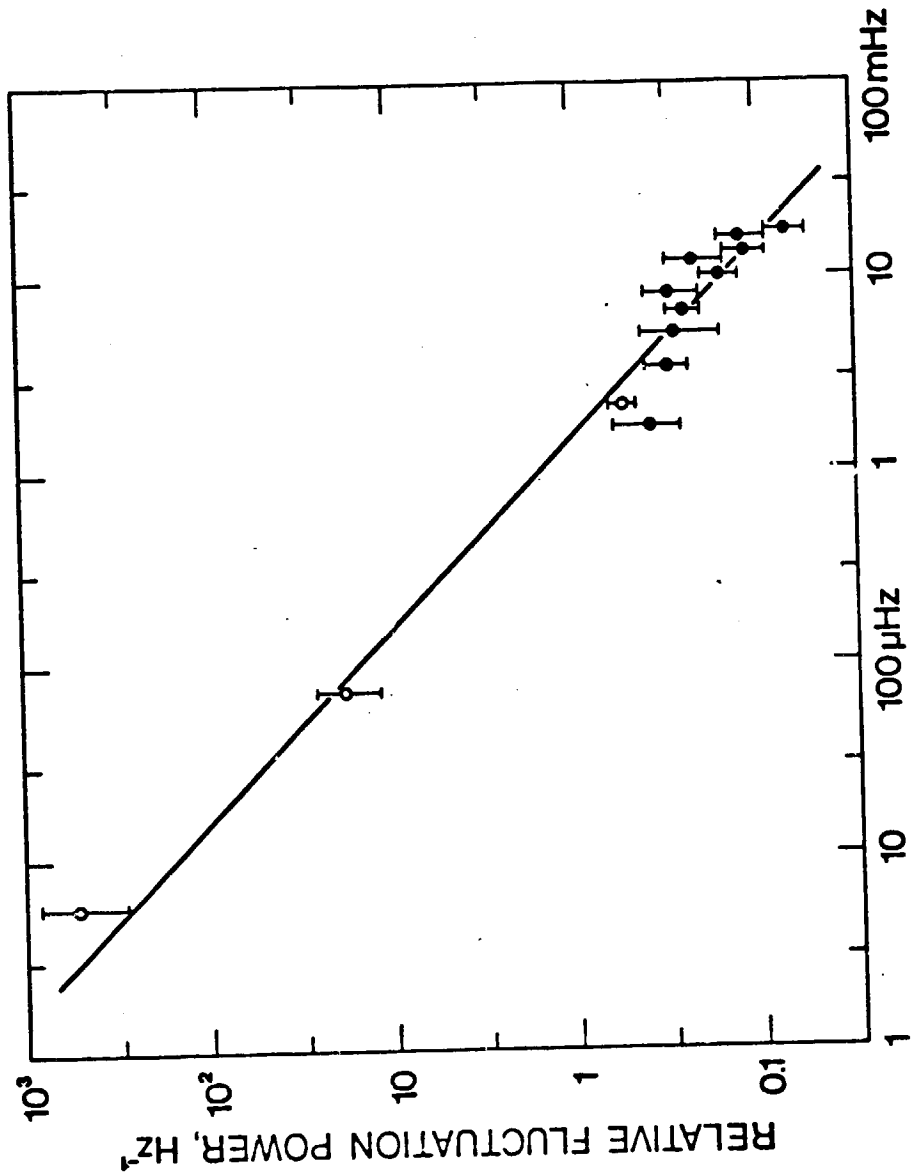

Fig. 10 . The power spectrum of the Io 4.8-μm fluctuations. The solid points are obtained from rapidly sampled data; the open circles are obtained from night-to-night and ~40-minute sampling with allowance made for aliasing. The line has a slope of -1.

that transport the internal heat to the surface by analogy with the transport of Ba atoms in the theory of BaO cathodes.

Sinton and Kaminski continued their observations of Io at the IRTF during eclipse by Jupiter and successfully observed 3 reappearances in June and July. The 10-μm results from 6 eclipses are shown in Figure 11 along with the 1980 observations of Morrison and Telesco. Similar data have been obtained at 20 μm. During the period just prior to re-emergence from eclipse, which is critical for heat flux measurement, Io was observed at 3.5, 4.8, 8.7, 12.5, and 30 μm as well. In Figure 12 we look at the mean fluxes in the 10-μm band during this critical period when >90% of the flux comes from the volcanoes. The data are plotted separately for each eclipse. The volcanic emission at 10 μm is remarkably constant, but if a change has occurred in the last two years, it most likely has been a decrease. The relative constancy at 10 μm is remarkably different from the variability found at 4.8 μm and lends credence to Sinton's flow model in which the 10-μm radiation arises from cooling old flows, while the 4.8-μm radiation comes from current activity (Sinton 1982).

A remarkable effect that is shown in Figure 11 cannot, now, be ignored in deriving the total heat flux from the volcanoes. The effect, noted in the 1970 work (Morrison 1977) is that the flux level approached asymptotically after eclipse is substantially below that observed before eclipse and counter to thermophysical models. We must understand the cause of this effect before we can derive a definitive value for the volcanic heat flux. Sinton, with the assistance of Tittemore, continued the program of computing thermophysical models of Io eclipses with ever increasing eloboration. Two years ago they began with flat-disk homogeneous models. They they went to spherical models and the calculation of the diurnal temperature gradients prior to imposition of the eclipse. The diurnal period is 42.5 hours, and an eclipse is about 4

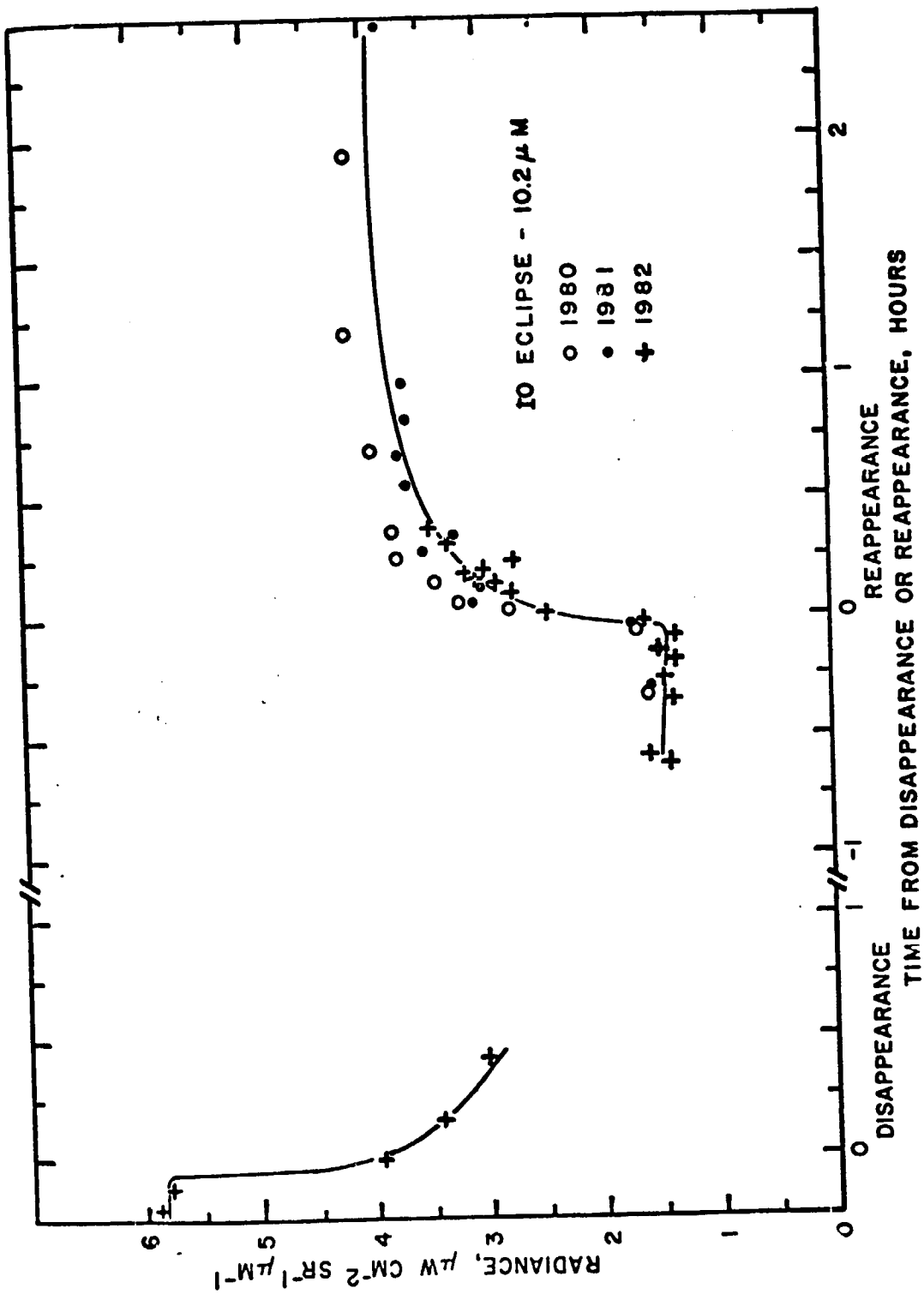

Fig. 11. Observations of eclipses of Io at 10-μm. The open circle points were obtained by Morrison and Telesco (1980) while the other points were obtained by Sinton and Kaminski.

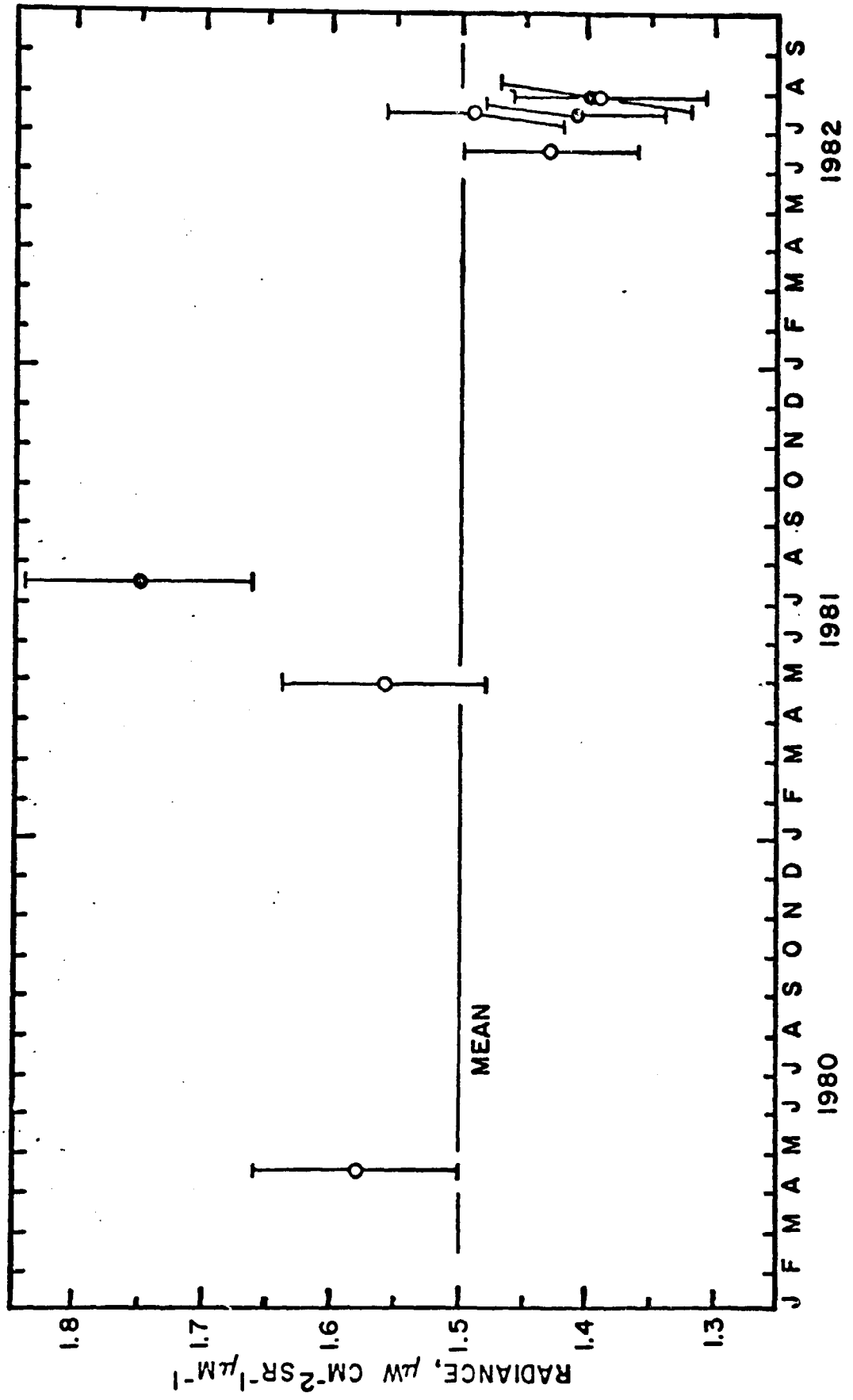

Fig. 12. Measurements of the Io flux in the 10-μm band immediately prior to emergence from eclipse. Open circles are data obtained in the broadband 10-μm filter. Solid points are obtained from weighted means of 8.7 and 12.5-μm data.

hours from start to recovery. The subsurface gradients depend on the square root of the ratio of the periods. Thus the diurnal-imposed thermal state is important to the correct calculation of the eclipse, and, indeed, important effects were found. Sinton realized that they may yet be ignoring an important factor, considering the aforementioned discrepancy shown in Figure 11 and they searched further. It was realized that rotation of Io during the eclipse was being left out of the calculation. During the dark phase, the rotation brings some night-chilled surface around from the back and removes some of the day-warmed subsurface. When reappearance occurs, the subsurface has a significantly different thermal state from that of a nonrotating Io. Figure 13 illustrates the detail of their present rotating model calculations. Figure 14 shows the flux variation at 20 μm for this model, and indeed a substantial difference between posteclipse and preeclipse fluxes is found. They are continuing the mathematical studies, and another important effect will be included in the modeling. The Voyager pictures of Io show that ~5% of the surface is covered with calderas with ~10% albedo. The material in the calderas is most likely a lava with a high thermal inertia, so the calderas cool only slightly during the eclipse. Because their albedos are low, they are substantially hotter than the majority of the surface and remain so during eclipse. Thus, they masquerade as the volcanic hot spots that we are trying to detect. At least 5 to 10% of the 10-μm flux during the total phase may be ascribed to the dark regions and is not volcanic heat flow. We are now calculating horizontally inhomogeneous models with all of the rotational and diurnal subsurface gradients included, but we have not yet been able to calculate a curve whose shape agrees with the entire variation shown in Figure 11. We believe that the observational program, which has been well supported by grants of substantial time on the IRTF, merits exhaustive modeling efforts before we derive a value for the volcanic heat flux from Io.

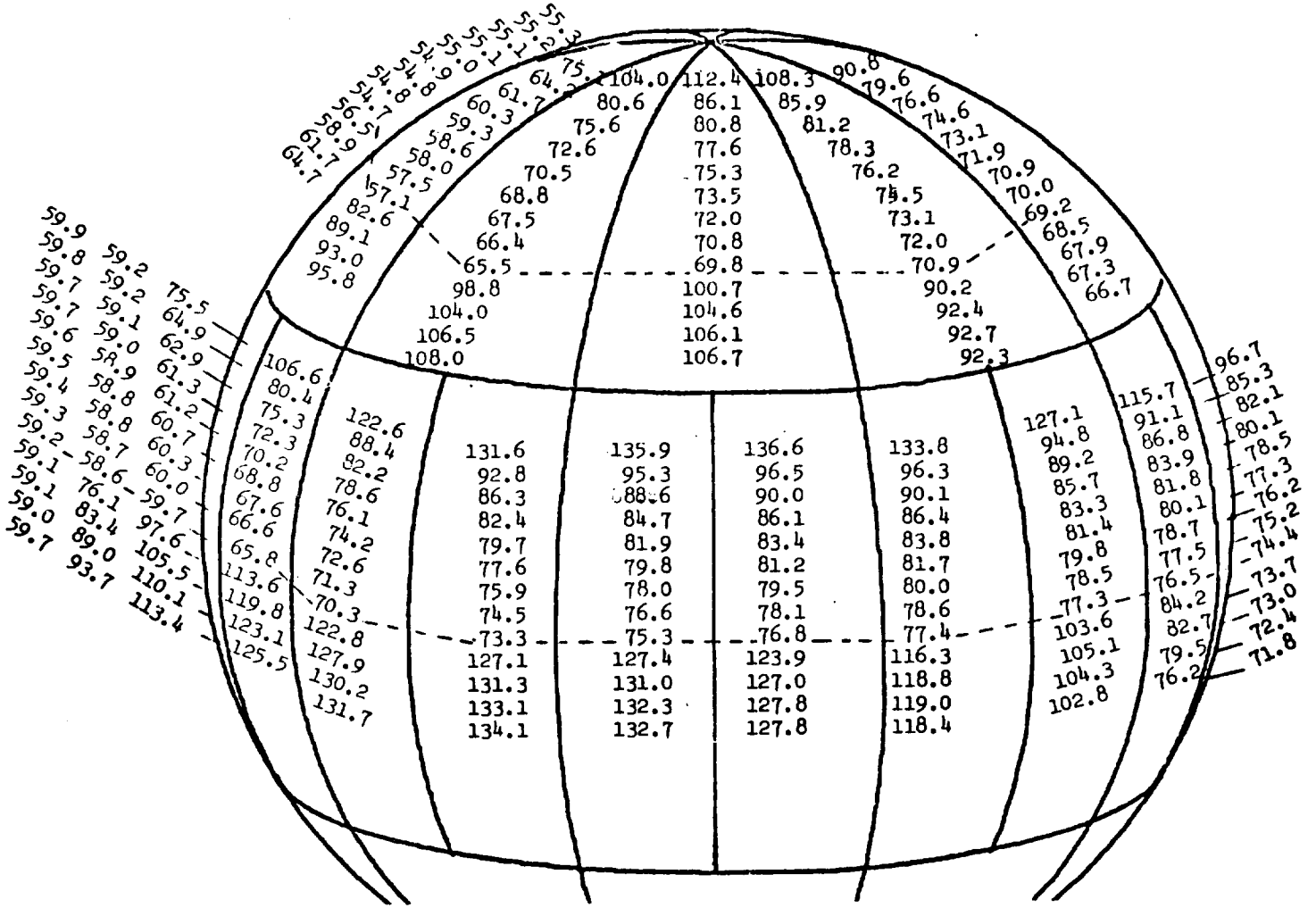

Fig. 13 Temperatures (K) of a rotating, homogeneous thermophysical model of Io with thermal parameter = 1.5×10^{-4}. The surface temperatures shown in each gore proceed from immediately prior to the eclipse until 1.1 hours after reappearance. The dashed lines connect the last temperature before reappearance. The meridians of the gores are as viewed from the sun at disappearance. As time progresses, each gore rotates to the right. For the equatorial band the amount of rotation is ~1-1/2 gore widths for the last temperature shown. Temperatures listed off of the disk on the left wrap around to the backside. Only every tenth temperature of those computed is shown.

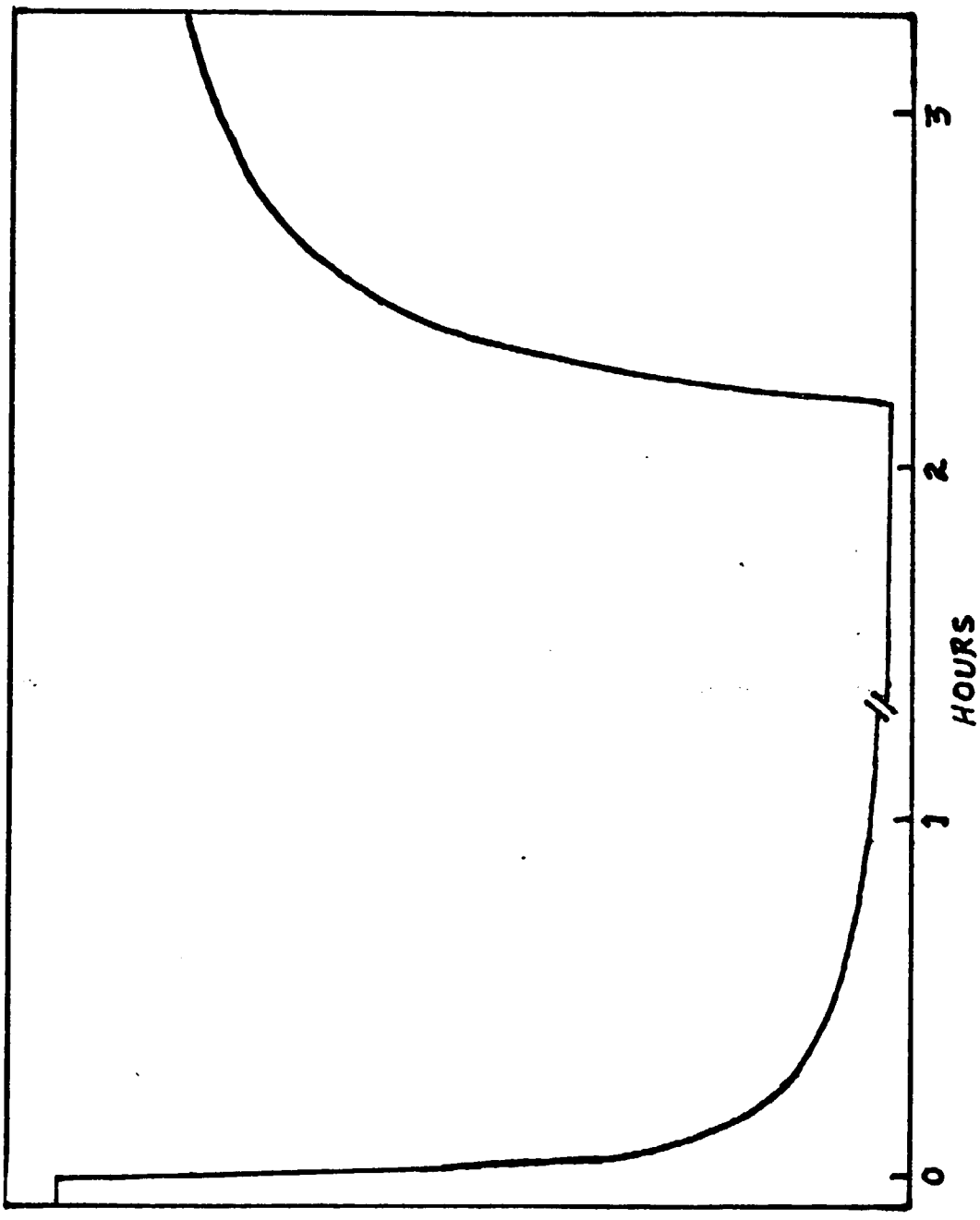

Fig.14 The 20-μm flux variation computed from the rotating homogeneous thermophysical model of Io illustrated in Fig. 13. The break in the middle of the curve occurs because the left of this the computation is for a phase angle 9° before opposition, while to the right it is for 9° after opposition. The model calculations show a substantial difference in the out-of-eclipse fluxes before and after eclipse.

5. Radiometric Determination of Satellite Diameters

The radiometric/photometric technique, which was pioneered in Hawaii, has proved the most valuable method for measuring the sizes and albedos of small airless bodies not accessible to direct spacecraft study. We report here the first measurements, made using this technique, of the sizes of the four largest satellites of Uranus, plus significant new constraints on the sizes of Triton and Pluto.

These new satellite diameters and albedos were obtained by R. H. Brown (also affiliated with the Planetary Geosciences group at the Hawaii Institute of Geophysics), Morrison, and Cruikshank while observing with the IRTF in May 1982. The large aperture, low background, and excellent site of the IRTF were critical for these measurements, which involved radiation at wavelengths between 20 and 30 μm. The results have been published in Nature, in one paper by Brown et al. on the Uranus satellites and a companion paper by Morrison et al. on the Triton and Pluto results.

The four brightest satellites of Uranus—Umbriel, Ariel, Oberon, and Titania--were each measured on two or more nights, permitting a final flux determination with uncertainties as small as ~±10%. Corrections for the transmission of the atmosphere in the long-wave part of the 20-μm band were achieved using measurements of extinction due to atmospheric water vapor made from infrared spectra obtained the same night. The measurements were interpreted using the new calibration of the radiometric technique derived during the past two years in Hawaii (Brown et al. 1982), together with new visual magnitudes for the satellites obtained by Goguen and Brown (reported elsewhere). The results are summarized in Table 1.

The Uranian satellites are seen to be larger, and to have lower albedos, than had generally been assumed before these measurements were made. The new

Table 1

Calculated diameters and albedos

Object	m_{20}	$V(0°)$	$V(1.0)$	q	Diameter (km)	p_v
Ariel	−1.78±0.22	1.03±0.05	1.3±0.2	0.8±0.1	1,330±130	0.30±0.06
Umbriel	−1.70±0.18	1.89±0.05	2.2±0.2	0.7±0.1	1,110±100	0.19±0.04
Titania	−2.41±0.14	0.91±0.05	1.2±0.2	0.7±0.1	1,600±120	0.23±0.04
Oberon	−2.53±0.17	1.10±0.05	1.4±0.2	0.7±0.1	1,630±140	0.18±0.04
Rhea	−3.54±0.06	—	0.24	1.02	1,530±45	0.60±0.04
Rhea	−3.53±0.06	—	0.24	1.02	1,530±45	0.60±0.04

m_{20} is the 20-μm monochromatic magnitude corrected to an Earth–object distance of 1 AU and 0° solar phase angle (assuming a brightening of 0.01 mag deg^{-1}). $V(0°)$ is the visual magnitude at 0° solar phase angle corrected to 1 AU from the Earth and Sun (see Text). $V(1, 0)$ is the $V(0°)$ with the opposition surge removed (see text), q is the assumed phase integral (except the value for Rhea taken from ref. 11). p_v is the visual geometric albedo. All errors are ± 1 s.d. of the mean, except those quoted for the assumed phase integrals and the $V(1, 0)$, which represent our estimates of a reasonable range of values.

albedos of ~20% are consistent with the "dirty ice" interpretation of their spectra (see elsewhere in this report). The new size and albedo values have been provided to the Voyager project to be used in planning imaging sequences and exposure values. This result thus qualifies as direct support for a flight project, as well as yielding important scientific results.

Observations made at the same time of Triton and Pluto yielded upper limits rather than detections. These upper limits represented significant improvements over previous values, however, permitting us to constrain the radii of both objects to the values given in Table I. Both objects appear to be similar, with sublunar dimensions and moderately bright surfaces with albedo ~0.4.

D. ASTEROIDS AND COMETS

1. Figures and Satellites of Asteroids

Goguen, with the help of K. Roselius, developed software and hardware to interface the Apple data system with SI-11 computer, enabling Apple data floppy disks to be copied to magnetic tape for return to Honolulu and detailed analysis on the main IFA Perkin-Elmer computer. Goguen began a long-term

project of asteroid photometry and observed three stellar occultations by solar system objects as detailed below.

Many asteroids exhibit large-amplitude, rapid variations in brightness due to their elongated shape and rotation. The observed rotational lightcurve varies as the asteroid and earth move in their orbits, i.e., with phase angle and viewing aspect. By observing lightcurves and developing a simple model that can reproduce all observed lightcurves and their major variations, it should be possible, with some assumptions, to determine shapes, pole orientations and surface photometric functions for several asteroids. A similar project is underway by Chapman and colleagues at PSI in Tucson with the main concentration on determining shapes. Our concentration will be on defining asteroid surface photometric functions, especially opposition effects, for different taxonomic types. Observations of the Tucson and Hawaii groups are being coordinated to minimize duplication of effort.

Another goal is to search for eclipse and transit features in asteroid lightcurves indicating the presence of a satellite body. Some lightcurves show a complex pattern that is not easily explained by a simple shape. Because eclipses and transits are mutual shadowing events, corresponding lightcurve minima should vary in a predictable fashion with phase angle, and should be distinguishable from single body minima. The magnitude of shadowing features will depend on the relative sizes of the two bodies and their separation. If a binary asteroid can be found and its separation and orbital period measured, the total mass of the pair is known. Currently, although asteroid sizes are well constrained, asteroid masses, and hence densities, are only poorly estimated.

The accompanying Figure 15 shows two nights of V photometry of 349 Dembowska. Compare the sharp minimum seen on September 19 to the smooth

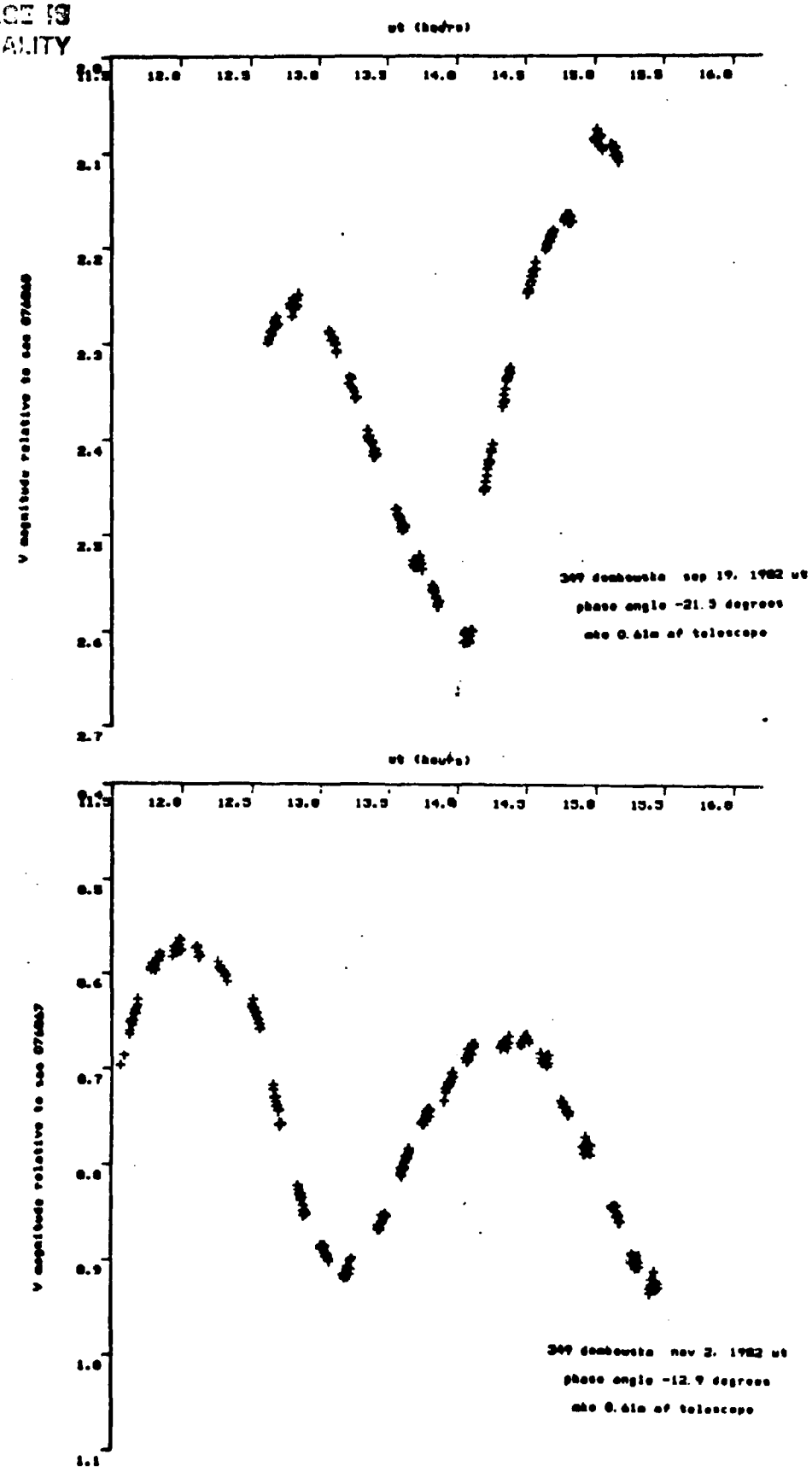

Fig. 15

minimum seen on November 2. During the report period, six asteroids were observed on 14 nights. G. Aldering assisted with some of the observing.

2. Near Occultation by a Comet

At the annual DPS meeting in Boulder, Colorado, L. Wasserman presented a poster talk on predicted occultations of stars by comets. On October 23 UT comet P/Churynmov-Gerasimenko (1982f) would occult ninth magnitude SAO 077190 with the "shadow" central line passing ~100 km from MKO. Since this was the most favorable predicted event and MKO was the best placed site, Goguen left the meeting to observe the event. V filter photometry with two-second resolution (21 km) shows the optical depth along the line of sight through the comet to be $\tau < 0.01$, i.e., less than the 1 σ precision of the data.

3. Photometry of Faint Comets, VJHK

Cruikshank, in collaboration with W. K. Hartmann and J. Degewij, has obtained new VJHK photometry of outer solar system (OSS) asteroids and satellites showing different broad surface classes such as clean ices, RD material, and C material can be distinguished by VJHK colors. This is confirmed experimentally by VJHK colorimetry of ices, soils, and dirty-ice mixtures prepared by R. N. Clark. As ice is added to these soil samples, their colors migrate across the VJHK diagrams from the "dark dirty" color fields toward "pure ice color fields" (Figure 16a).

All of the eight comets observed so far have colors generally resembling RD asteroid surfaces and inconsistent with clean ice surfaces such as those of Europa or Rhea. Some color variations on a time scale of days, possibly involving particle size effects, were observed. Of special interest is the RD-like color (somewhat displaced toward the icy field) of comet P/Schwassmann-Wachmann 1 at quiescence, when the nucleus may have been observable. These observations suggest but do not prove the presence of RD-like dust (dirty ice,

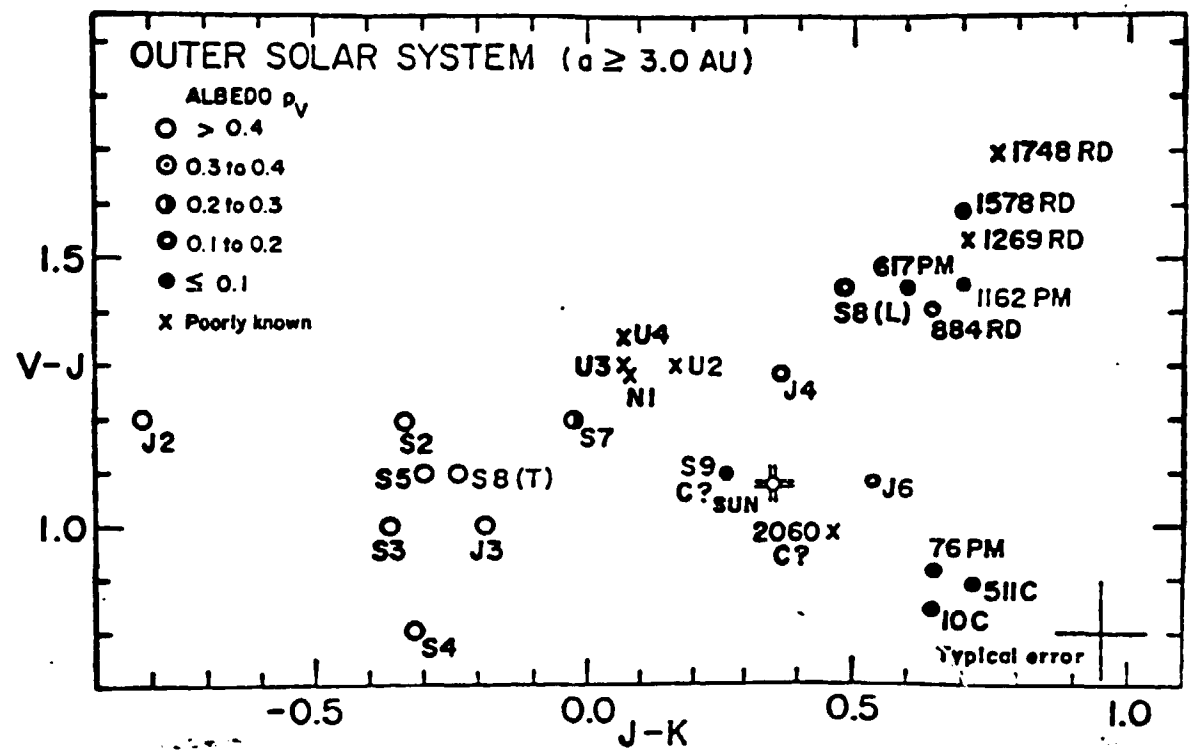

Fig. 16a

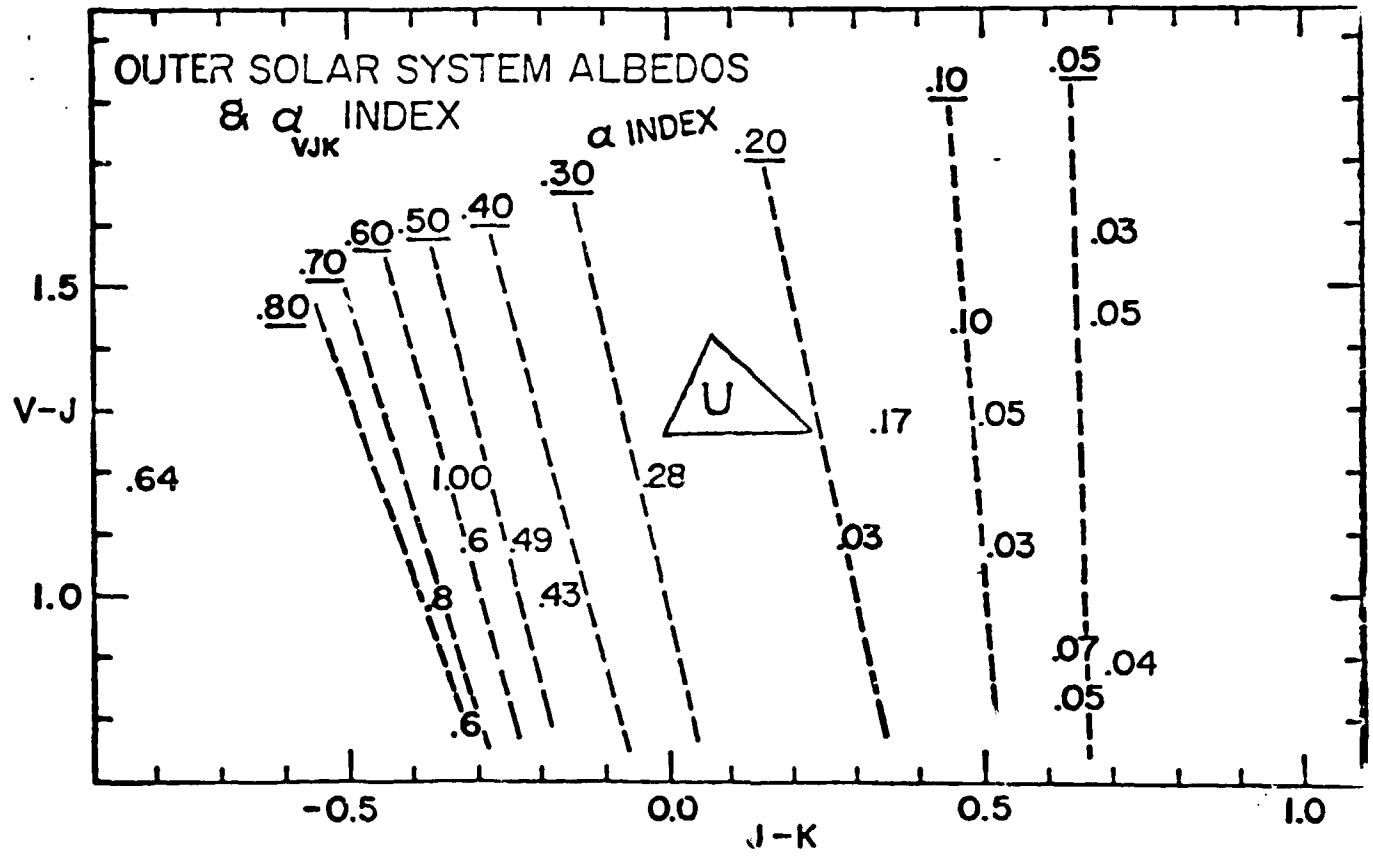

Fig. 16b

colored by RD-like dust in these comets. Coloring effects due to particle size, dispersal, and composition need further study.

We have proposed a two-component mixing model involving ices and dark dust as major constituents of OSS interplanetary bodies and outer planet satellites. Based partly on this model, we derived from VJHK colors an "α index" which correlates well with albedo and ice dust ratio on observed asteroids and satellites (Figure 16b). We note a correlation of α index with heliocentric distance for comets, suggesting plausible depletion of the ice component in coma material along close-in comets (Fig. 17).

Cruikshank is continuing the observations of faint comets and specific OSS asteroids for the purpose of confirming the relationships already identified, particularly for the comets, as this may provide a means of understanding the nature of the dusty component and its evolution with cometary activity. This work involves additional VJHK photometry, and eventually circular variable filter spectrophotometry throughout the range accessible to us with the new 0.8-2.6-μm system.

E. OTHER RESEARCH ACTIVITY

1. Laboratory Studies of Ices

In connection with the unidentified spectral feature at 2.15 μm in the spectrum of Triton, Cruikshank has collaborated with R. H. Brown and R. Clark of the HIG Planetary Geosciences Division in a laboratory study of the ices of methane, ethylene, ethane, and nitrogen. The frosts and ices were prepared in an environment chamber designed and constructed for this work and the spectra were obtained with a CVF spectrometer designed and built by Clark. Data were obtained from 0.6-2.5 μm. Additional spectra of methane frost in the 0.9-μm region were obtained with a grating spectrometer and Vidicon detector on loan to Cruikshank from J. M. Pasachoff of Williams College.

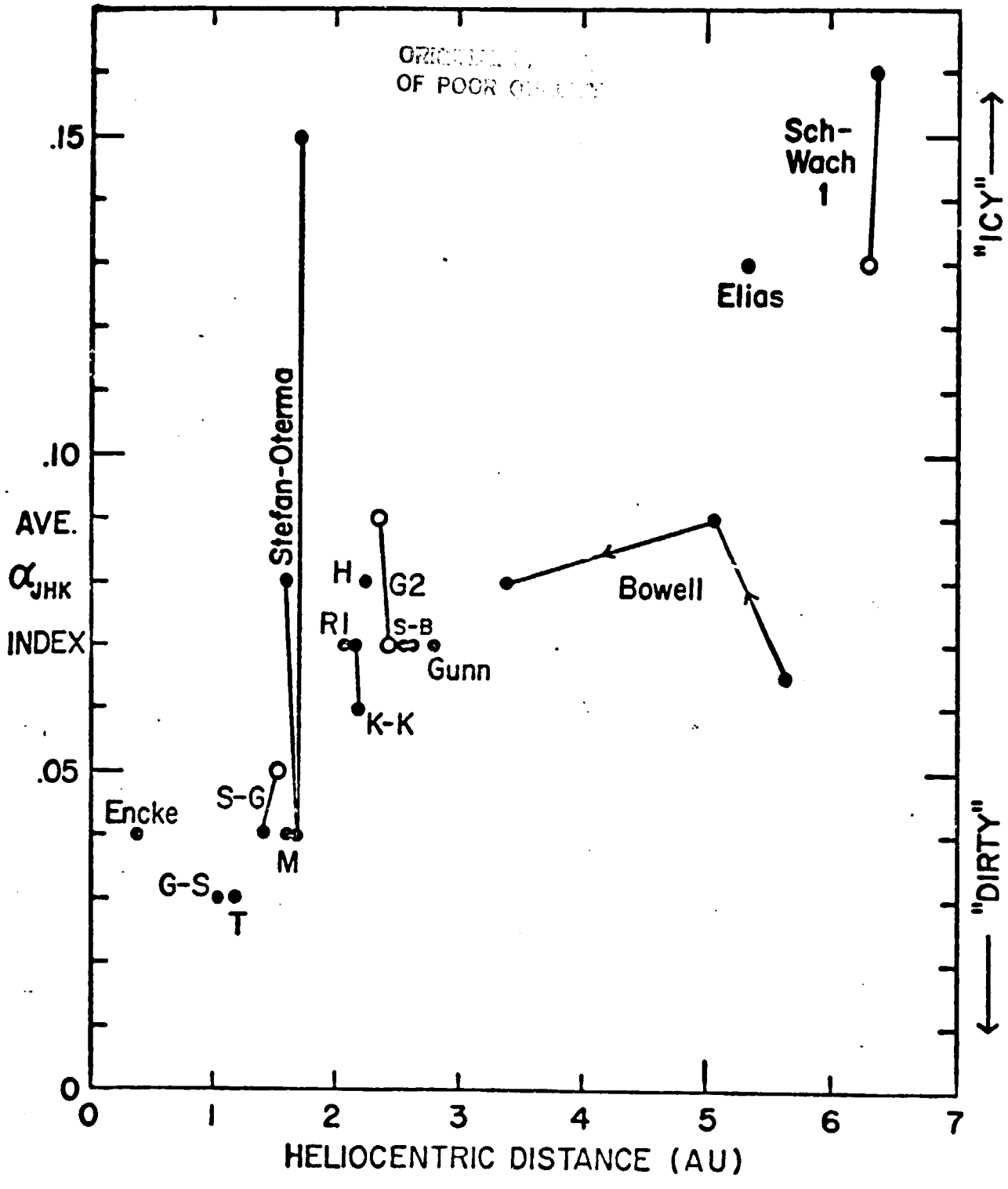

Fig. 17

The infrared spectra of methane, ethane, and ethylene are very rich with strong absorption features, some of which are candidates for a fit to the Triton spectrum, though the abundances of the higher hydrocarbons ethane and ethylene are expected to be 10^{-6} or 10^{-7} with respect to methane on Triton. The spectrum of liquid and solid nitrogen in this region is very neutral with no distinct absorptions, as expected from the fact that nitrogen is a homonuclear molecule.

Because there are no spectra of these compounds in the literature for comparison with planetary surfaces and atmospheres, Brown, Cruikshank, and Clark propose to publish the new data.

2. Speckle Interferometry

The ideal detector for speckle interferometry at visible wavelengths would be a device which determined the location and arrival time of each photon. Such a device, a MultiAnode Microchannel Array or MAMA, has recently been developed by G. Timothy of the University of Colorado. He, working with researchers at the University of Hawaii, has used a one-dimensional version for spectroscopy at Mauna Kea and a two-dimensional (256 x 1024) version will soon be available.

Howell has constructed an interface between the electronics provided by Colorado and the UH 2.24-m telescope data system and expects to use the detector for several speckle projects in the summer of 1983. As an initial, simple project, he intends to conduct a survey of asteroids to determine if the controversial reports of binary and multiple objects are in fact real. Most of those reports have come from stellar occultations, which are by their very nature unrepeatable. Some speckle work on asteroids has been presented by the speckle group at Steward Observatory, but those results are also controversial. The excellent seeing at Mauna Kea, combined with the advantages of the new detector, should allow a resolution of this problem.

Most planetary applications of speckle interferometry require not just measurements of the visibility function (or equivalently the autocorrelation of the image) but rather true reconstruction of the image. Various methods have been proposed such as the Knox-Thompson and Feinup algorithms, but to date the astronomical results have been disappointing. One reason that has been suggested for this is the nonideal nature of the detectors used (typically some type of intensified TV camera followed by a conventional video recorder). Unfortunately, the process of discriminating photon events with such systems can add noise and systematic errors. The MAMA detector should allow us to investigate the reconstruction algorithms without the confusion caused by these added problems.

Time tagging of the photons also allows more conventional forms of "image stabilization" to be carried out after the data are recorded. If there is a point source or other suitable reference in the field, then it is possible to shift the position of the photon events as they are later coadded to form the image. One can then remove the effects of image wander at any frequency up to a limit set by the brightness of the reference. At IFA, J. Heasley is interested in developing such processing capabilities,and they should allow subarcsecond images of Uranus and Neptune to be made.

In October Howell implemented an infrared speckle interferometry system on the CFH telescope and obtained observations of T Tauri. They help to define the spectra and color temperature of the optical star and the infrared companion which was first discovered by Dyck, Simon, and Zuckerman this past year. Their discovery explains several peculiarities of this rather untypical "prototype" of the T Tauri class of stars, in particular its excess infrared and its radio emission. The companion may in fact represent an intermediate case between stellar and planetary formation and therefore clearly deserves further study.

The CFHT IR speckle system should prove to be especially powerful because it is the largest telescope on Mauna Kea and has excellent optical image quality. Therefore it allows one to take advantage of the good seeing that can occur. As an example, Figure 18 shows the four best scans out of 200 of the infrared triple ζ Aqr, the main components of which are separated by only 1.2 arcseconds.

This separation is comparable to the diameter of the disk of Io and suggests the observations of it that should be possible. Io is known to undergo outbursts where its brightness increases by factors of three, and such scans could show the location of the outburst. Speckle processing should also show the number and location of faint hot spots. Such observations have up to now been prevented by various problems with implementing the speckle system on the large telescopes here. Some problems still remain with the CFHT system, but if they can be eliminated we hope to observe Io in the spring of 1983.

2. 3.8- and 4.8-μm Standard Stars

The circumsky coverage of CIT standard stars, mentioned in the previous semiannual report (#24), was completed. To the original list of 45 stars we have added several additional A0V stars at magnitude 5 to 6, which brings the total list to 48 stars. We now include about 8 stars in the range B9V to A1V to improve the connection to the photometric systems at other wavelengths. At the moment we have not decided whether we will make this connection via α Lyr, defined $\equiv$ 0.00 magnitude, or to float its magnitude and make the mean A0V colors $\equiv$ 0.00. We will make this decision after consultation with IR observers at the Institute.

A problem was encountered with the gain steps of the lock-in amplifier provided at the 2.24-m telescope. Virtually at the completion of observing,

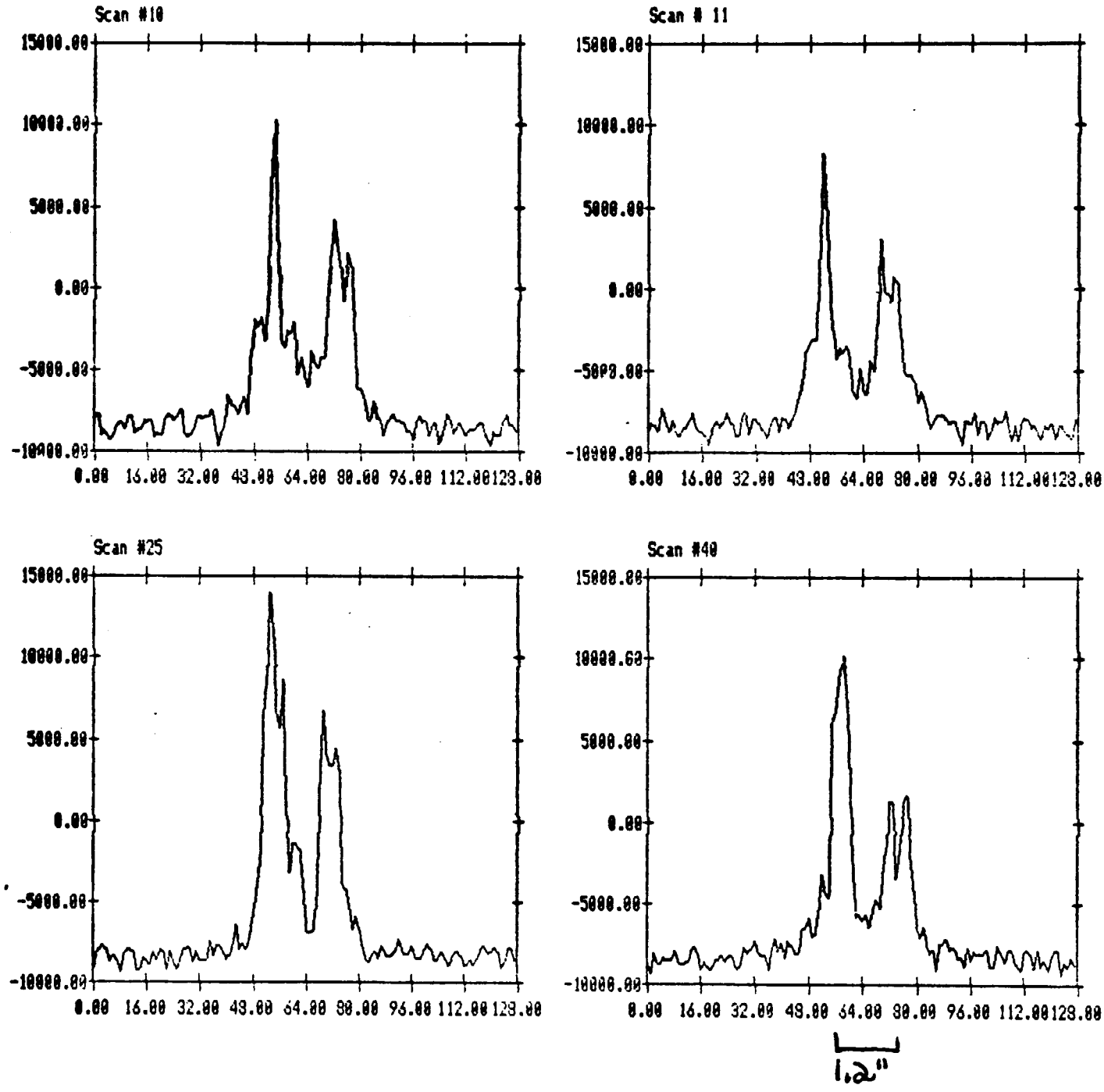

Fig. 18. Four best scans out of 200. Ir triple.

we discovered that three of the amplifier gain settings were off by 10-25% from their calibrated values, and worse, they were variable from night to night. This problem did not afflict the Io monitoring data, for Io and a sufficient number of calibration stars were observed at reliable gain steps. The amplifier problem does introduce an uncertainty into the standard star program. We will probably need to reobserve a number of stars to reach a dependable magnitude system for all stars.

4. Eclipse of ε Aurigae

The F0Ia supergiant ε Aurigae is eclipsed every 27 years by an object whose nature is mysterious. The duration and depth of the eclipse (Kopal, Astrophys. and Space Sci. 10, 332, 1971) are inconsistent with the passage of any solid body with a circular cross-section across the primary star. The indicated shape is a long bar or edge-on disk (e.g., Huang, Astrophys. J. 141, 976, 1965). Visual spectroscopy reveals Doppler shifts of the primary's absorption lines consistent with the influence of a secondary having about 10 $M_\odot$ (Morris, J. R. Astron. Soc. Canada 56, 210). The implied size for this body would be about 9 AU along its orbit.

The present eclipse began in July 1982 and will continue through January 1984. We obtained broadband infrared measurements from 1-20 μm and CVF spectra (~1% resolution) from 1-5 μm prior to and during eclipse ingress. The eclipse depth is the same at all wavelengths from visual to 5 μm, but is less deep at 10 and 20 μm (see Fig. 19). The emission at 10 and 20 μm during eclipse yields a color temperature of 600 K for the flux from regions not obscured by the secondary (Backman et al., IAU Circular #3763, 1983). The luminosity is consistent with a blackbody of the size necessary to produce the eclipse at that same temperature. Thus, the measured temperature is likely to be that of the secondary. The spectra analyzed so far reveal no new absorptions appearing with the eclipse.

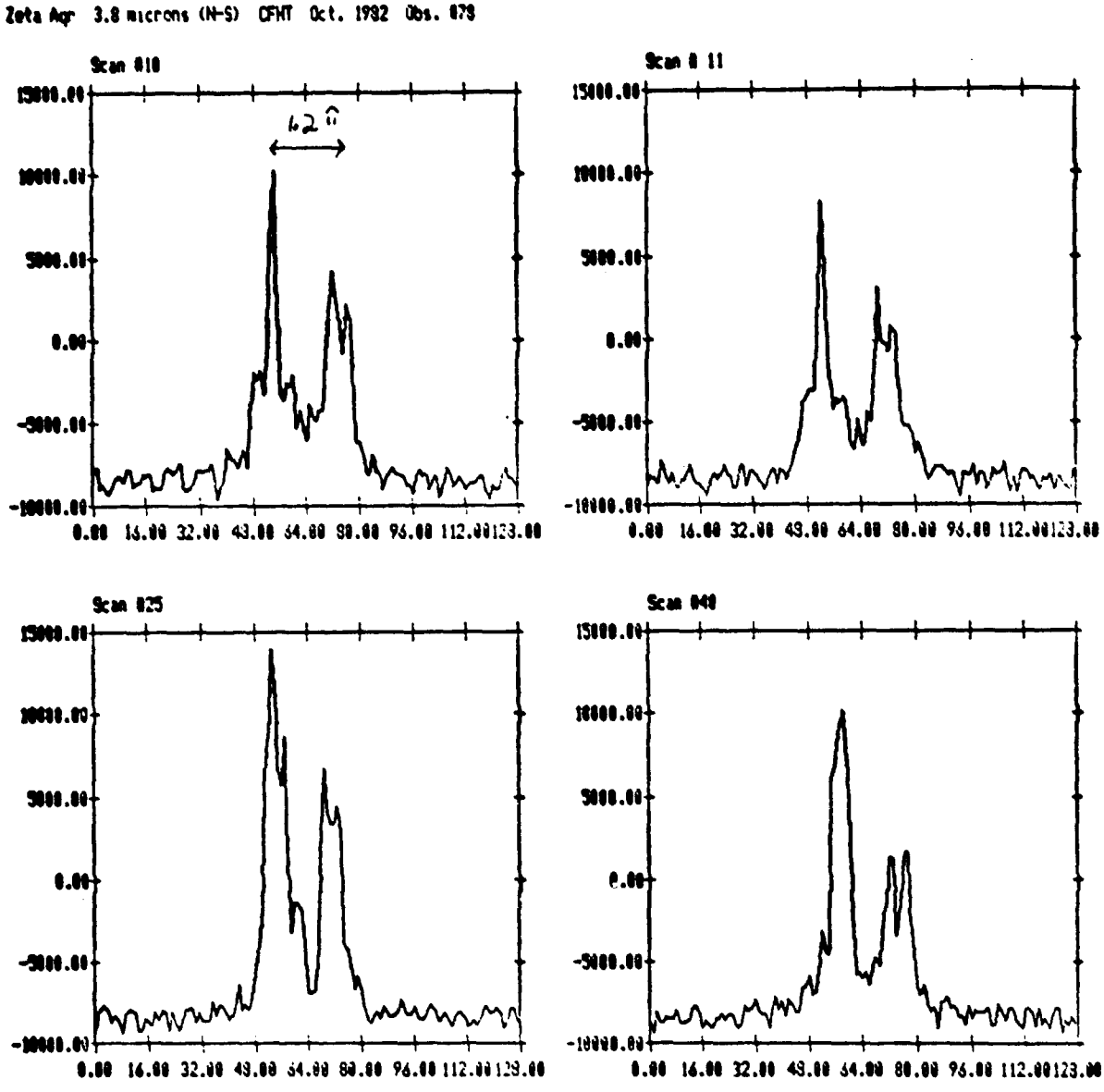

Fig. 19

Zeta Aqr is a visual double with a separation of 1.2 arcseconds in the North-South direction. The B component has a low mass, infrared companion. This figure presents the 4 best scans out of 200.

The ε Aurigae system is 10^7 years old or less (Stothers, Nature 229, 180, 1971). The cool temperature for the eclipsing object found through out infrared measurements, along with its shape, suggests a protoplanetary system seen edge-on. Furthermore, the temperature is so low that it is likely that any central secondary mass is not luminous because the energy input from the primary is enough to heat the secondary's material to at least that temperature. We may be observing a very early stage in planetary system/stellar formation.

Further studies are being made by us at Kitt Peak with 4-m FTS spectra, and collaborators have obtained UV spectra using IUE. The high-resolution spectra may allow modeling of the radiative transfer in this system and a more firm determination of its nature. In particular, emission lines are appearing in the core of Mg II H+K and Hydrogen Brackett-gamma (2.17 μm).

III. OTHER TOPICS

1. Cruikshank was elected Secretary-Treasurer of the Division for Planetary Sciences of the American Astronomical Society by the DPS committee at its meeting in Boulder in October 1982. He will serve for three years in this capacity.

2. Pilcher's planned 1983-1984 sabbatical at the University of Vienna was approved by the Austrian government.

3. Pilcher continued to serve on the Galileo Imaging Team and as an elected committee member of the AAS/DPS.

4. Cruikshank continued as an Associate Editor of Icarus, and as a member of the Board of Directors of the Canada-France-Hawaii Telescope Corp.

5. Morrison completed his one-year term as Chairman of the Division for Planetary Sciences of the AAS.

6. Morrison served on the Solar System Exploration Committee of NASA, and has been asked to become Chairman of the SSEC in 1983.

7. Ten years ago, Sinton used funds from this grant to take a composite photograph of Uranus and its five satellites at 8850 Å. Because of the interest generated by the coming Voyager encounter with Uranus, this photograph has attracted attention. Sinton has been filling an average of a request a month for copies of the picture for articles, textbooks, and other monographs.

8. Morrison continued his spacecraft activities as a member of the Voyager Imaging Team and as a Galileo Interdisciplinary Scientist.

9. Morrison began a two-year term as President of the Astronomical Society of the Pacific.

10. Morrison participated in the International Astronomical Union

meeting in Greece and attended the IAU Colloquium on Planetary Rings held in France immediately following the IAU.

11. Morrison completed work on the volume Satellites of Jupiter, which was published in November by the University of Arizona Press. This 972-page book, with 57 authors, has received a major fraction of Morrison's efforts during the past two years.

12. Morrison and J. Burns (Cornell) are co-organizers of an international meeting (IAU Colloquium No. 77) on the Natural Satellites to be held in Ithaca in July 1983. Cruikshank also serves as a member of the Organizing Committee. Following the meeting, a major book on the satellites, edited by Morrison and Burns, will be published by the University of Arizona Press.

13. Morrison is collaborating with T. Owen (SUNY) in writing an undergraduate text in planetary science. Publication is scheduled for 1984.

IV. BOOKS AND PAPERS PUBLISHED OR SUBMITTED IN 1982

A. PUBLISHED

R. H. Brown, D. P. Cruikshank, and D. Morrison. Diameters and Albedos of the Satellites of Uranus. Nature 300:423-425.

R. H. Brown, D. Morrison, C. M. Telesco, and W. Brunk. 1982. Calibration of the Radiometric Asteroid Scale Using Occultation Diameters. Icarus 52:188-195.

D. P. Cruikshank. 1982. Barnard's Satellite of Jupiter. Sky Telesc. 64:220-224.

D. P. Cruikshank. 1982. The Satellites of Uranus. In Uranus and Outer Planets, G. E. Hunt, ed. (London: Cambridge University Press), pp. 193-210.

D. P. Cruikshank and R. H. Brown. 1982. Surface Composition and Radius of Hyperion. Icarus 50:82-7.

D. P. Cruikshank. 1982. Spectroscopy of Triton and Pluto: Status and Prospects. In Vibrational-Rotational Spectroscopy for Planetary Atmospheres, M. J. Mumma et al., eds. NASA Conference Publication 2223, pp. 699-706.

R. A. Hanel + 12 other authors (including D. P. Cruikshank). 1982. Infrared Observations of the Saturnian System from Voyager 2. Science 215:544-548.

R. J. Hlivak, C. B. Pilcher, R. R. Howell, A. J. Colucci, and J. P. Henry. 1982. The Galileo/Institute for Astronomy Charge-Coupled Device System. Instrumentation in Astronomy IV, S.P.I.E. Proceedings, vol. 331, pp. 96-103.

J. S. Morgan and C. B. Pilcher. 1982. Plasma Characteristics of the Io Torus. Astrophys. J. 253:406-421.

D. Morrison. 1982. Introduction to the Satellites of Jupiter. In Satellites of Jupiter, D. Morrison, ed. (Tucson: University of Arizona Press), pp. 3-43.

D. Morrison, ed. 1982. Satellites of Jupiter. (Tucson: University of Arizona Press), 972 pp.

D. Morrison. 1982. The Satellites of Jupiter and Saturn. Ann. Rev. of Astron. and Astrophys. 20:469-495.

D. Morrison. 1982. Voyages to Saturn. NASA SP-451, 227 pp.

D. Morrison and D. P. Cruikshank. 1982. The Outer Solar System. In The New Solar System, 2nd ed., J. K. Beatty, B. O'Leary, and A. Chaikin, eds. (Cambridge, MA: Sky Publishing Corp.), pp. 167-176.

D. Morrison, D. P. Cruikshank, and R. H. Brown. 1982. The Diameters of Triton and Pluto. Nature 300:425-427.

D. E. Osterbrock and D. P. Cruikshank. 1982. Keeler's Gap in Saturn's A Ring. Sky Telesc. 64:123-126.

J. C. Pearl and Sinton, W. M. 1982. Hot Spots of Io. In Satellites of Jupiter, D. Morrison, ed. (Tucson: University of Arizona Press), pp. 724-755.

C. B. Pilcher and D. F. Strobel. 1982. Emissions from Neutrals and Ions in the Jovian Magnetosphere. In Satellites of Jupiter, D. Morrison, ed., (Tucson: University of Arizona Press), pp. 807-845.

W. M. Sinton. 1982. Io: A Volcanic Flow Model for the Hot Spot Emission Spectrum and a Thermostatic Mechanism. Icarus 51:563-573.

W. M. Sinton. 1982. Telescope. McGraw-Hill Encylopedia of Science and Technology, vol. 13, 5th ed., pp. 533-535.

B. A. Smith et al. (including D. Morrison). 1982. A New Look at the Saturn System: The Voyager 2 Images. Science 215:504-537.

B. IN PRESS

R. A. Brown, C. B. Pilcher, and D. F. Strobel. 1983. Spectroscopic Studies of the Io Torus. In Physics of the Jovian Magnetosphere, A. J. Dressler, ed. (Cambridge: Cambridge University Press), in press.

R. H. Brown and D. P. Cruikshank. 1982. The Uranian Satellites: Surface Compositions and Opposition Surges. Icarus, submitted.

D. P. Cruikshank, J. F. Bell, M. J. Gaffey, R. H. Brown, R. Howell, C. Beerman, and M. Rognstad. 1982. The Dark Side of Iapetus. Icarus, in press.

D. P. Cruikshank. 1982. The Development of Studies of Venus. In Venus, D. M. Hunten, and L. Colin, eds. (Tucson: University of Arizona Press), in press.

W. K. Hartmann, D. P. Cruikshank, and J. Degewij. 1982. Remote Comets and Related Bodies: VJHK Colorimetry and Surface Materials. Icarus, in press.

D. Morrison. 1983. Outer Planet Satellites. Rev. Geophys. Space Phys., in press.

E. J. Shaya and C. B. Pilcher. 1983. Polar Cap Formation on Ganymede. Icarus, submitted.

W. M. Sinton, F. C. Cheigh, D. Lindwall, and W. Tittemore. 1983. The Io Near-Infrared Monitoring Program, 1979-1981. Icarus, in press.

W. M. Sinton. 1983. On Io All That Flickers Is Not Cold. Icarus, submitted.

P. Thomas, J. Veverka, D. Morrison, T. Johnson, M. Davies, and B. Smith. 1983. Phoebe: Voyager 2 Observations. J. Geophys. Res., in press.

P. Thomas, J. Veverka, T. Johnson, D. Morrison, and B. Smith. Voyager Observations of the Small Satellites of Saturn. J. Geophys. Res., in press.

V. OPERATION OF THE 2.24-M TELESCOPE

A. TELESCOPE UTILIZATION

Statistics relating to the usage of the 2.24-m telescope are presented in the accompanying table. During 1982, the telescope was used on all clear nights, with a negligible amount of time lost to failure of the telescope, data acquisition computers, or other systems maintained by observatory staff. This high level of reliability is particularly noteworthy since electronics technicians are normally not available during nights or weekends to make repairs.

During 1982, slightly 42% of the observing time was devoted to planetary programs. Half of those observations were carried by members of the Institute for Astronomy staff. The remaining planetary time was used by members of T. B. McCord's group at the University of Hawaii's Institute for Geophysics and by visitors.

B. PROGRESS REPORT--2.24-M TELESCOPE

During the past year, we have continued to make progress in developing electronic detector systems for the 2.24-m telescope. An intensified Reticon system, which is well suited for spectroscopy of faint objects, is now in regular use. This system was constructed at the Institute for Astronomy with support from NSF and the State of Hawaii. There have been several observing runs with the Galileo CCD system, and subarcsecond images have been obtained of objects as faint as R(mag)=25. The testing and operation of this detector are supported jointly by NASA and the State of Hawaii. Finally, we use the multianode microchannel array detectors developed by Gethyn Timothy with NASA support.

We have continued to develop software for the 2.24-m telescope control system and to upgrade the data acquisition system. Support scientist W. Heacox has taken responsibility for the development of software. We have

improved the computer slew, raster scanning, offset, and beamswitch capabilities of the 2.24-m telescope. We now have a CAMAC-based data acquisition system with software that appears to the user to be identical to that in use at the IRTF. With NSF support, we have acquired a tape drive and a Winchester-type fixed disk for the data acquisition system. We hope soon to replace the LSI 11 in the data acquisition system with an LSI 11/23. The expansion in memory from 28 K to 256 K that this change would permit is essential to allow on-line processing of data obtained with array detectors.

2.24-M TELESCOPE USAGE - 1982

Observer	No. of Nights (Planetary)	No. of Nights (Nonplanetary)
Backman	19.1	
Boesgaard		1.0
Bonsack		5.5
Christian		3.5
Cruikshank	18.5	
Dyck		8.0
Goguen	14.5	
Heasley		11.2
Henry		21.3
Howell	6.5	
Impey		18.5
Morgan	2.5	
Morrison	5.0	
Pilcher	11.8	
Rose		21.0
Simon		4.3
Sinton	22.0	
Stockton		16.8
Telesco		2.0
Thompson		8.7
Tully		5.0
Wolff		
Visitors	15.0	57.6
HIG	34.1	
Total	149.0 (42%)	202.0 (56%)

Engineering: 8.0 (2%)